Draft Manuscript for Review

Geochemical evolution of arc and slab following subduction initiation: a record from the Bonin Islands, Japan

Journal:	*Journal of Petrology*
Manuscript ID	JPET-Feb-20-0021.R2
Manuscript Type:	Original Manuscript
Date Submitted by the Author:	27-Apr-2020

Complete List of Authors:	Ishizuka, Osamu; National Institute of Advanced Industrial Science and Technology Geological Survey of Japan, Taylor, Rex; University of Southampton Faculty of Natural and Environmental Sciences Umino, Susumu; Kanazawa University Graduate School of Natural Science and Technology Kanayama, Kyoko; Tottori Prefecture

Keyword:	subduction initiation, boninite, geochemistry, Bonin Islands, Izu-Bonin-Mariana arc

Geochemical evolution of arc and slab following subduction initiation: a record from the Bonin Islands, Japan

Osamu Ishizuka*

Institute of Earthquake and Volcano Geology, Geological Survey of Japan, AIST, Central 7, 1-1-1, Higashi, Tsukuba, Ibaraki, 305-8567, Japan. e-mail address: o-ishizuka@aist.go.jp Phone: +81-29-861-3828, Fax: +81-29-856-8725

Also at: Japan Agency for Marine-Earth Science and Technology, 2-15 Natsushima, Yokosuka, Kanagawa, 237-0061, Japan

Rex N. Taylor

School of Ocean and Earth Sciences, University of Southampton, Waterfront Campus, Southampton, SO14 3ZH, UK. E-mail: rex@soton.ac.uk

Susumu Umino

Division of Natural System, Kanazawa University, Kanazawa, Ishikawa 920-1192, Japan. E-mail: sesumin@staff.kanazawa-u.ac.jp

Kyoko Kanayama

Tottori Prefecture, Iwami, Tottori, 681-0001, Japan E-mail: kanayamak@pref.tottori.lg.jp

Running title: Arc magma evolution after subduction initiation

*corresponding author

ABSTRACT

Volcanism following the initiation of subduction is vital to our understanding of this specific magma-generation environment. This setting is represented by the first development of the Izu-Bonin-Mariana arc system as subduction commenced along the Western Pacific margin in the Eocene. A new collection of volcanics recovered from the islands and exposed crustal sections of the Bonin Ridge span the first 10 Myr of arc evolution. An elemental and radiogenic isotope dataset from this material is presented in conjuction with new $^{40}Ar/^{39}Ar$ ages and a stratigraphic framework developed by a detailed mapping campaign through the volcanic sections of the Bonin Islands.

The dating results reveal that both the locus and type of magmatism systematically changed with time in response to the progressive sinking of the slab until the establishment of steady-state subduction at around 7-8 Myr. Following initial MORB-like spreading-related basalt magmatism, volcanic centres migrated away from the trench and changed from high-Si boninite to low-Si boninite/high-Mg andesite, then finally tholeiitic/calcalkaline arc magma.

Subducting pelagic sediment combined with Pacific-type igneous ocean crust dominate the slab input to the shallow source of high-Si boninites at 49 Ma, but high-precision Pb isotope data show that this sediment varies in composition along the subducting plate. At around 45 Ma, volcanism switched to low-Si boninite and the pelagic sediment signature was almost entirely replaced by volcanic or volcaniclastic material originating from a HIMU ocean island source. These low-Si boninites are isotopically consistent with a slab component comprising variable proportions of HIMU volcaniclastics and Pacific MORB. In turn, this signature was replaced by a Pacific MORB-dominated flux in the post 45 Ma tholeiite and calcalkaline volcanics. Notably, each change in slab-derived flux coincided with a change in the magma type.

Fluctuations in the slab-derived geochemical signature were superimposed on a change in the mantle wedge source from highly-depleted harzburgite to a depleted MORB-type mantle-type source. In turn, this may correspond to the increasing depth of the leading edge of the slab through this 5 Myr period.

Key words: subduction initiation; boninite; geochemistry; Bonin Islands; Izu-Bonin-Mariana arc

INTRODUCTION

Subduction initiation and the subsequent development of oceanic island arcs are poorly understood and remain an important unresolved problem in plate tectonics (e.g., Stern, 2004). Stern *et al.* (2012) emphasized the importance of studying forearc sections, which are not masked by younger sediment or accreted material from the subducting plate, to elucidate processes at subduction initiation. Recent geological and geophysical surveys of the trenchward Izu-Bonin-Mariana forearc, in sections such as the Bonin Ridge and SE of Guam, have revealed that their crustal stratigraphy was generated during the initial stages of arc formation (e.g., Ishizuka *et al.*, 2006a, 2011a, 2014a; Reagan *et al.*, 2010, 2017). These forearc crustal sections span ~1200 km along the arc, yet have quite consistent stratigraphic sequences, which from bottom to top are: 1) gabbroic rocks, 2) a sheeted dyke complex, 3) basaltic lava flows, 4) lava flows, dykes and volcaniclastics of boninite and tholeiitic andesite, and 5) tholeiitic and calcalkaline basalt to andesite. In addition to the crustal section, dredge sampling and ROV dives recovered mantle peridotite beneath the gabbro. These observations indicate that almost all of the forearc crust down to Moho has been preserved in this forearc area.

Based on these subaerial and submarine studies of the trenchward forearc, processes at subduction initiation have to some extent become clearer. Subduction along the Izu-Bonin-Mariana arc is estimated to have initiated at c. 52 Ma. The onset of slab sinking and the associated counterflow of asthenospheric mantle resulted in seafloor spreading on the overriding plate, which generated the first volcanism in the form of forearc basalts (FAB: Reagan *et al.*, 2010). These eruptions are followed at ~46-50 Ma by boninitic magmatism, and then tholeiitic and calcalkaline magmatism at ~44-45 Ma. A comprehensive record of the boninitic and subsequent early arc tholeiitic to calcalkaline arc magmatism is preserved and exposed on the Bonin Islands (Umino, 1985; Umino & Nakano, 2007; Umino *et al.,* 2009, 2016; Kanayama *et al.*, 2012, 2014).

This outline model for subduction initiation described above needs to be tested by determining the nature and composition of the subduction-derived material and the local sub-crustal mantle during the magmatic development. Taylor *et al.* (1994) showed that boninites from the Chichijima Island have uniquely low Sm/Zr and Ti/Zr, and along with other geochemical characteristics of boninites, they implied that slab melts with residual amphibole might contribute to boninite magma as well as a variably depleted mantle source. Kanayama *et al.* (2012) also found that the same processes generated the boninites from the Mukojima Islands. Umino *et al.* (2015, 2018) analysed primitive melt inclusions in chrome spinel and recognised two types of boninite magma. Temperature-pressure conditions for primary boninites, which range from 1345°C at 0.56 GPa to 1421°C at 0.85 GPa for the 46–48 Ma low-

Si and high-Si boninites, and 1381°C at 0.85 GPa for the 45 Ma low-Si boninite. They suggested that at 46–48 Ma, introduction of slab fluids induced melting of the residue of preceding basaltic magmatism (FAB) and high-temperature harzburgite, resulting in the low-Si and high-Si boninites, respectively. By 45 Ma, convection within the mantle wedge brought the less-depleted residue of FAB and depleted MORB-type mantle (DMM) into the region fluxed by slab fluids, which melted to yield the less-depleted low-Si boninite, and more fertile arc basalts, respectively.

The composition of early arc magmatism is also a function of the proportions and nature of components added from the slab; such components may change as subduction progresses. To unravel the temporal admixtures of mantle and subduction components therefore requires a comprehensive elemental and isotopic dataset of volcanics that span the established stratigraphic framework of early arc magmatism. This contribution presents new geochemical dataset as well as $^{40}Ar/^{39}Ar$ ages for samples from the entire volcanic history of the Bonin Islands. These data are used to establish the geochemical evolution of early arc magmatism, and investigate the processes operating during the establishment of a new subduction zone.

GEOLOGICAL BACKGROUND

The Izu-Bonin arc marks the eastern margin of the Philippine Sea plate and is formed by westward subduction of the Pacific plate (Fig. 1a). This arc extends from southern Honshu to the south of Io-to Island, and continues further south as the Mariana arc. Izu-Bonin arc has a broad volcanic zone extending in an east-west direction and is bounded by the Izu-Ogasawara Trench to the east and the Shikoku Basin to the west. Between 25^{o}N and 29^{o}N, there is a prominent N-S trending forearc massif called the Bonin Ridge in an area between the Quaternary volcanic front and Izu-Ogasawara Trench (Fig. 1a,b). The Bonin Ridge is separated from the volcanic front by the Ogasawara Trough, which rifted in the Eocene or Oligocene (Fig. 1b; Taylor, 1992; Ishizuka *et al.*, 2006a). This preserved the Bonin Ridge as an intact terrain without any effects from later overlapping magmatism.

The subaerial Bonin Ridge

Bonin Islands sit atop an uplifted segment of the Bonin Ridge and expose a sequence of the early Izu-Bonin arc volcanism (Fig. 2). The islands are geographically divided into 3 groups (Fig. 1b): Mukojima Island Group (northern Bonin Islands), Chichijima Island Group (central Bonin Islands) and Hahajima Island Group (southern Bonin Islands). The boninitic sequence, known as the Maruberiwan Formation, is the stratigraphically lowest unit exposed on the Bonin islands (Fig. 2). This unit includes boninite, bronzite andesite, dacite and rhyolite (Umino, 1985; Umino & Nakano, 2007), and is exposed on the Chichijima Island Group as well as the Mukojima Island Group. Maruberiwan Formation boninites mostly classify as high-Si boninite (Kanayama *et al.*, 2012) and were formed in the Eocene between 46-48 Ma (Cosca *et al.*, 1998; Ishizuka *et al.*, 2006a, 2011a). A quartz-bearing dacite-rhyolite sequence (Asahiyama Formation; Umino, 1985) unconformably overlies the Maruberiwan Formation, however, no significant time gap exists between the Asahiyama Formation and underlying boninitic rocks (45.8 Ma: Ishizuka *et al.*, 2011a). The youngest volcanics on the Chichjima Island Group are the lavas and clastics of the Mikazukiyama Formation. These high-Mg two-pyroxene andesites and low-Si boninites (Kanayama *et al.*, 2012) unconformably overlie the rhyolites of the Asahiyama Formation (Fig. 2; 44.3-44.74 Ma).

Tholeiitic to calcalkaline basaltic to andesitic rocks from Hahajima Island Group are the youngest volcanic sequence exposed on any of the Bonin Islands (Fig. 2; Taylor & Nesbitt, 1995; Ishizuka *et al.*, 2006a; Kanayama *et al.*, 2014; Umino *et al.*, 2016). An $^{40}Ar/^{39}Ar$ age of 44.0 ± 0.3 Ma has been reported for an andesite lava from Hahajima (Ishizuka *et al.*, 2006a).

Submarine section of the Bonin Ridge

A recent investigation of the submarine section east of the Bonin Ridge has expanded the forearc stratigraphy to beneath that exposed on the Bonin Islands (Ishizuka *et al.*, 2011a). This was found to consist of basalt lava flows and basaltic sheeted dykes, which were named forearc basalt (FAB) solely based on their current geographic location (Reagan *et al.*, 2010). $^{40}Ar/^{39}Ar$ dating of these forearc basalts indicate an age between 48 and 52 Ma (Ishizuka *et al.*, 2011a). This predates the boninites and implies that the first magmatism following subduction initiation was produced at around 52 Ma. Zircon U-Pb ages of gabbro are 51.6 and 51.7 Ma, respectively, suggesting that the FAB and gabbros are co-magmatic (Ishizuka *et al.*, 2011a).

Li et al. (2013) reported low-Ca (high-Si) boninite from Hahajima Seamount (ESE of Hahajima Island: Fig. 1b) with a $^{40}Ar/^{39}Ar$ age of 44 ± 1.4 Ma. They argued that genesis of boninite involves melting of subducted volcaniclastic sediments derived from a HIMU seamount and Pacific slab as well as depleted Indian MORB-type mantle.

IODP Exp. 352 drilled in the Bonin forearc and recovered both forearc basalt and boninite at different Sites (Reagan *et al.*, 2017, 2019; Shervais *et al.*, 2019). The forearc basalt section reconfirmed that FAB magmatism initiated at around 52 Ma (Reagan *et al.*, 2019). Geochemical characteristics of the FAB imply that two stages of melting took place to produce FAB magma (Shervais *et al.*, 2019). First stage melting is estimated to have occurred in the garnet stability field, probably hundreds of millions of years before subduction initiation (Yogodzinski *et al.*, 2018). Second stage melting is estimated to be of a larger degree, occurring at higher temperature and lower pressure (1400-1480^{o}C, 1-2 GPa) compared to that for N-MORB.

Drilling also revealed that low-Si boninite erupted at 51.3 Ma with a clear slab-derived signature (Li et al., 2019). Based on these results, Reagan *et al.* (2019) concluded that FAB magmatism lasted for a short period of around 0.7 Myr. Subsequent supply of a slab-derived flux initiated boninite magmatism from melting of the depleted mantle residue after FAB extraction.

Spatial variation of volcanism

Forearc basalts are found on the inner trench wall of the Izu-Ogasawara Trench, i.e., the easternmost volcanic sequence in this area. A high-Si boninitic sequence younger than 48 Ma occurs on the shallower slope of the inner trench wall, i.e., west of the forearc basalts and on the Bonin Islands. Post-44 Ma tholeiitic and calcalkaline lavas are exposed along the western escarpment of the Bonin Ridge, just west of the Bonin Islands where boninites occur, as well as on the Hahajima Islands (Ishizuka *et al.*, 2006a). Thus, based on these observations, the locus of volcanism appears to have moved westward, i.e. away from the trench, with time (Ishizuka *et al.*, 2011a). This may be related to the progressive establishment of subduction and a well-defined mantle wedge (e.g., Stern, 2004; Ishizuka *et al.*, 2006a, 2011a). Extension of the overriding plate at subduction initiation might have controlled the location of the forearc basaltic volcanism (e.g., Stern & Bloomer, 1992; Hall *et al.*, 2003), and then cooling of the mantle wedge by the sinking slab, counter flow of asthenospheric mantle, and initiation of slab dehydration/melting all could have affected the focus of volcanism after 48 Ma (e.g., Ishizuka *et al.*, 2006a).

SAMPLES STUDIED

Samples used in this study were mainly collected during geological mapping campaigns on the Bonin Islands (Umino & Nakano, 2007; Umino *et al.*, 2009, 2015). They are representative of all subaerially exposed volcanics, and cover the entire age-range of magmatism exposed on the Bonin Islands (Fig. 2). High-Si boninite series rocks (Kanayama et al., 2012) were collected from the Mukojima Island and Chichijima Island Groups, reported in this contribution as Mukojima and Chichijima groups, respectively. Transitional high-Mg cpx-opx andesites and low-Si boninites (Kanayama et al., 2012) of the Mikazukiyama Formation were collected from Chichijima and Otoutojima, and described as Mikazukiyama group. Other younger basaltic to andesitic rocks were collected from the Hahajima Island Group (reported as Hahajima group). Exact sample localities are listed in Tables S1-S5. For some of the samples from Mukojima, Chichijima and Hahajima Island Groups, whole rock chemical compositions have been published in Taylor *et al.* (1994), Kanayama *et al.* (2012, 2014) and Ishizuka *et al.* (2014b).

The samples used for analyses were selected from the much larger number of samples collected during the mapping campaign. Sample selection was mainly based on microscopic observation of thin sections and, in some cases, stereomicroscopic observation of rocks. Criteria for sample selection were; 1) The sample should mostly retain fresh groundmass, 2) Most of the phenocrysts are fresh, 3) Free from secondary mineral crystallisation (e.g., zeolites, opal) inside vesicles.

Specifically for $^{40}Ar/^{39}Ar$ dating, only high-Si boninites, which retain pristine glassy groundmass, were chosen. For samples from the Mikazukiyama group and Hahajima group, those with relatively crystalline groundmass composed of mainly plagioclase and pyroxene with only minor amounts of fresh interstitial glass were selected.

ANALYTICAL PROCEDURES

Whole rock chemistry

About 20 g of rock chips were ultrasonically cleaned with distilled water, and then crushed with an iron pestle and pulverised using an agate mortar. Whole rock major elements were analysed on glass beads, prepared by fusing 1:10 mixtures of 0.5 g subsamples and lithium tetraborate. The glass beads were analysed using a Panalytical Axios XRF spectrometer at the Geological Survey of Japan/AIST. External uncertainty and accuracy are generally <2% (2.s.d), but Na could have as much as ~7% analytical uncertainty. The data for each element are in agreement with accepted values and uncertainties of international standards (Table S1).

The rare-earth elements (REE), V, Cr, Ni, Rb, Sr, Y, Zr, Nb, Cs, Ba, Hf, Ta, Pb, Th and U concentrations were analysed by ICP-MS on a VG Platform instrument and Agilent 7900, both at the Geological Survey of Japan/AIST. About 100 mg of powder from each sample was dissolved in a HF-HNO_3 mixture (5:1) using screw-top Teflon beakers. After evaporation to dryness, the residues were re-dissolved with 2% HNO_3 prior to analysis. In and Re were used as internal standards, while JB2 with a similar level of dilution to the samples was used as an external standard during ICP-MS measurements. Instrument calibration was performed using 5-6 calibration solutions made from international rock standard materials (including BIR-1, BCR-1, AGV-1, JB1a, BEN). Reproducibility is generally better than ±4% (RSD) for the REE, and better than ±6% (RSD) for other elements except those with very low concentration and Ni (see BHVO2 analysis in Table S1). Detection limits vary from element to element, but for elements with low concentrations, such as REE and Ta, limits typically fall within a range from 0.2 to 2 pg g^{-1}.

Radiogenic isotopic composition

Isotopic compositions of Sr, Nd, and Pb were determined on 500 mg of hand-picked 0.5–1mm rock chips. The chips were leached in 6M HCl at 140°C for 20-30 minutes prior to dissolution in HF-HNO_3. Sr, Nd and Pb isotope ratios were measured on a nine-collector VG Sector 54 mass spectrometer. Sr was isolated using Sr resin (Eichrom Industries, Illinois, USA). For Nd isotopic analysis, the REE were initially separated by cation exchange, before isolating Nd on Ln resin (Eichrom Industries, Illinois, USA) columns. Procedural Sr and Nd blanks were considered negligible relative to the amount of sample analysed. Sr and Nd isotopic compositions were determined as the average of 150 ratios by measuring ion beam intensities in multi-dynamic collection mode. Isotope ratios were normalised to $^{86}Sr/^{88}Sr$ = 0.1194 and $^{146}Nd/^{144}Nd$ = 0.7219. Measured values for NBS SRM-987 and JNdi-1 (Tanaka *et al.*, 2000) were $^{87}Sr/^{86}Sr$ = 0.710278 ± 19 (2 s.d., n =33) and $^{143}Nd/^{144}Nd$ = 0.512104 ± 10 (2 s.d., n = 38) during the measurement period. All $^{87}Sr/^{86}Sr$ ratios were normalised to NBS SRM-987 $^{87}Sr/^{86}Sr$ = 0.710248 (Thirlwall, 1991), and $^{143}Nd/^{144}Nd$ ratios were normalised to JNdi-1= 0.512115 (Tanaka *et al.*, 2000) as measured during the same analytical session.

The Pb isotopic compositions were determined at the Geological Survey of Japan/AIST and University of Southampton, UK. Average isotope ratio data from both laboratories was found to be within ~1 s.d., and were within similar levels of uncertainty of the poly-spike SRM 981 values of Taylor et al., (2015). Consequently data presented are not internally adjusted or normalised. At the Geological Survey of Japan/AIST, Pb separation was achieved using AG1-X8 200-400 mesh anion exchange resin. Procedural Pb blanks were <30pg, and considered negligible relative to the amount of sample analysed. Pb isotopic measurements were made in multi-dynamic collection mode using the double spike technique (Southampton-Brest-Lead 207-204 spike SBL74: (Ishizuka *et al.*, 2003; Taylor *et al.*, 2015)). Natural (unspiked) measurements were made on 60-70 % of collected Pb, giving ^{208}Pb beam intensities of 2.5-3 × 10^{-11}A. Fractionation-corrected Pb isotopic compositions and internal errors were obtained by a closed-form linear double-spike deconvolution (Johnson & Beard, 1999). The reproducibility of Pb isotopic measurements (external error: 2 s.d.) by double spike is <200 ppm for all $^{20x}Pb/^{204}Pb$ ratios. Measured values for NBS SRM-981 during the measurement period were

$^{206}Pb/^{204}Pb$=16.9407 ± 0.0039, $^{207}Pb/^{204}Pb$=15.5010 ± 0.0050, and $^{208}Pb/^{204}Pb$=36.724 ± 0.012 (2 s.d., n = 21).

At the University of Southampton, rocks were prepared for Pb isotope analysis by initially crushing inside a plastic envelope using a non-torque press. Crushed material was then separated to 0.5-1.0 mm using a Teflon sieve set. This fraction was repeatedly cleaned with in ultra-pure water in an ultra-sonic bath. Cleaned rock-chips were then picked during microscopic examination. Samples were leached for 30-40 min in 4M HCl at 200°C prior to Pb separation using HBr-HCl anion exchange columns. Lead isotope ratios were measured by a Thermo Neptune MC-ICP-MS at the University of Southampton UK, using a double spike run of each sample to correct for instrumental mass fractionation. The ^{207}Pb-^{204}Pb SBL74 spike was added such that $^{204}Pb_{sample}/^{204}Pb_{spike}$ was 0.09 ±0.03. Procedural blanks range between 50-100 pg Pb. NBS SRM 981 values achieved during the measurement period were $^{206}Pb/^{204}Pb$ = 16.9406 ±0.0030, $^{207}Pb/^{204}Pb$ = 15.4980 ±0.0030, $^{208}Pb/^{204}Pb$ = 36.7188 ±0.0086 (2s.d.; n = 17).

The Hf isotope ratios were measured on a Thermo Neptune MC-ICP-MS at the University of Southampton, UK. Hf isotope ratios were monitored and corrected for mass fractionation using $^{179}Hf/^{177}Hf$ = 0.7325 and for interferences using the values reported in Chu *et al.* (2002). Hf isotopes are reported relative to $^{176}Hf/^{177}Hf$ of JMC 475 of 0.282158. Repeated JMC 475 measurements during the measurement period gave $^{176}Hf/^{177}Hf$ = 0.282161 ± 0.000010 (2s.d.; n = 26).

$^{40}Ar/^{39}Ar$ dating

Ages of the fresh volcanic rocks were determined using the $^{40}Ar/^{39}Ar$ dating facility at the Geological Survey of Japan/AIST. Details of the procedures are reported in Ishizuka *et al.* (2009, 2018). 20-25 mg of phenocryst-free groundmass, crushed and sieved to 250 – 500 µm in size, was analysed using a stepwise heating procedure. The samples were treated in 6N HCl for 30 minutes at 95°C with stirring to remove any alteration products (clays and carbonates) present in interstitial spaces. After this treatment, samples were examined under a microscope. Sample irradiation was done at the JRR3 and JRR4 reactors for 24 hours except for the sample 06062604C irradiated at the CLICIT facility of the Oregon State University TRIGA reactor for 4 hours. Sanidine separated from the Fish Canyon Tuff (FC3) was used as flux monitor and assigned an age of 27.5 Ma, which has been determined against the primary standard for our K-Ar laboratory, Sori biotite, the age of which is 91.2 Ma (Uchiumi & Shibata, 1980).

A CO_2 laser heating system (NEWWAVE MIR10-30) was used in continuous wave mode for sample heating. A faceted lens was used to obtain a 3.2 mm-diameter beam with homogenous energy distribution to ensure uniform heating of the samples during stepwise heating analysis. Argon isotopes were measured on a VG Isotech VG3600 noble gas mass spectrometer fitted with a BALZERS electron multiplier except for sample 06062604C, which was measured on an IsotopX NGX noble gas mass spectrometer fitted with a Hamamatsu Photonics R4146 secondary electron multiplier in a peak-jumping mode.

Correction for interfering isotopes was achieved by analyses of CaF_2 and $KFeSiO_4$ glasses irradiated with the samples. The blank of the system including the mass spectrometer and the extraction line was 7.5×10^{-14} ml STP for ^{36}Ar, 2.5×10^{-13} ml STP for ^{37}Ar, 2.5×10^{-13} ml STP for ^{38}Ar, 1.0×10^{-12} ml STP for ^{39}Ar and 2.5×10^{-12} ml STP for ^{40}Ar with the VG3600 instrument, and 2.9×10^{-14} ml STP for ^{36}Ar, 1.4×10^{-13} ml STP for ^{37}Ar, 1.0×10^{-14} ml STP for ^{38}Ar, 1.2×10^{-14} ml STP for ^{39}Ar and 1.9×10^{-12} ml STP for ^{40}Ar with the NGX mass spectrometer. Blank analyses were done every 2 or 3 step analyses. All errors for ^{40}Ar/^{39}Ar results are reported at one standard deviation. Errors for ages include analytical uncertainties for Ar isotope analysis, correction for interfering isotopes, and J value estimation. An error of 0.5 % was assigned to J values as a pooled estimate during the course of this study. Results of Ar isotopic analyses and correction factors for interfering isotopes are presented in the supplementary data (Table S6).

Plateau ages were calculated as weighted means of ages of plateau-forming steps, where each age was weighted by the inverse of its variance. The age plateaus were determined following the definition by Fleck *et al.* (1977). Inverse isochrons were calculated using York's least-squares fit, which accommodates errors in both ratios and correlations of errors (York, 1969).

RESULTS

^{40}Ar/^{39}Ar ages

Six samples from the Hahajima group and one low-Si boninite from the Mikazukiyama group were dated by ^{40}Ar/^{39}Ar (Table 1; Fig. 3). Three samples from Hahajima gave ages between 40.2 and 45.28 Ma. For one sample (10093001-1), ^{36}Ar/^{40}Ar intercept of an inverse isochron plot does not agree with the atmospheric ratio within 2σ error. However, this is because the data points form a tight cluster near the radiogenic end of the plot, and the ^{36}Ar/^{40}Ar intercept is not well constrained. The weighted average of ages of 13 steps can be regarded as a reliable eruption age for this sample. The ages from the Hahajima Island are stratigraphically consistent (Umino *et al.*, 2016), i.e., two older samples (42.66 and 45.28 Ma) are from the lowermost Higashidai Formation and the youngest age (40.2 Ma) is from the uppermost Sekimon Formation (Fig. 2). Three Hahajima group samples from other islands of the Hahajima Island

Group gave ages between 38.4 and 44.6 Ma, which are overlapping or slightly younger than the ages from the Hahajima Island. Two samples (05122110 and 10092707-1) do not satisfy the definition of "age plateau" in a strict sense. For these samples, higher temperature steps which show decreasing ages as applied heating temperature increases appears to have been affected by recoil, but lower to middle temperature steps show constant ages and seem to be free from that effect. The weighted averages of the consecutive steps giving identical ages are adopted as best estimate for the eruption ages, which are consistent with regional stratigraphy.

A low-Si boninite of the Mikazukiyama group from the Otoutojima island of the Chichijima Island Group gave an age of 45.16 Ma, which is identical to the ages of cpx-opx andesites from the same formation within the 2σ uncertainty (Ishizuka *et al.*, 2006a, 2011a).

Major element compositions

Volcanics from the Bonin Islands show mainly andesitic/intermediate SiO_2 contents with some minor differentiated rocks including dacite and rhyolite, with basaltic rocks only present in the Hahajima group. Each volcanic group defines a distinct compositional range and trend on major element plots (Fig. 4). For example, taken at 8 wt% MgO, boninites from Mukojima and Chichijima have the highest SiO_2 (58-60 wt%), Hahajima group the lowest SiO_2 (50-55 wt%), with the cpx-opx andesites from the Mikazukiyama group at an intermediate level (Fig. 2, 4a). Mukojima and Chichijima boninites can be categorized as high-Si boninite (Kanayama et al., 2012).

In the Mikazukiyama group, boninites are the low-Si variety, whereas the cpx-opx andesites in this group have higher SiO_2 and lower MgO than the boninites (Fig. 4a). Boninite series rocks are absent in the Hahajima group, and instead both tholeiitic and calcalkaline basalts to andesites are present (Fig. 4b).

TiO_2 and CaO also show distinct trends among the different units. CaO and TiO_2 at a given MgO are lowest in the high-Si boninites, moderate in the low-Si boninites and cpx-opx pyroxene andesites in the Mikazukiyama group, and highest in the Hahajima group (Fig. 2, 4c,d).

Trace element compositions

Trace element ratios associated with fluid-mobile element enrichment are distinct among the different volcanic units. All volcanics from the Bonin Islands show significantly lower Ce/Pb relative to N-MORB (24.3: Gale et al., 2013: Fig. 5a) and most of the OIB (10-40: Willbold and Stracke, 2006). High-Si boninites from the Chichijima and Mukojima groups show the lowest Ce/Pb, while the Hahajima group shows the highest (Fig. 5a). Mikazukiyama group shows slightly higher Ce/Pb than the high-Si boninites except for highly differentiated samples, which have Ce/Pb >10, and among the Mikazukiyama group, cpx-opx andesites generally have lower Ce/Pb (1.5-3) than low-Si boninite (3-11). Other fluid-mobile elements such as Ba show a similar variation in enrichment among the different volcanic units. For example, volcanics from the Bonin Islands show significantly higher Ba/Nb relative to N-MORB (around 10: Gale et al., 2013) and comparable or higher than OIB (4 -25: Willbold and Stracke, 2006). Ba/Nb ratios are the highest for the high-Si boninites (30-130: Fig. 5b), while the Hahajima group shows the lowest Ba/Nb (10-50). The Mikazukiyama group again shows intermediate ratios between the high-Si boninites and the Hahajima group (mostly 20-90), and cpx-opx andesites show higher Ba/Nb than low-Si boninites.

Th enrichments yield different characteristics compared to those of the fluid-mobile elements. Th/Ce or Th/Nb (not shown) ratios are relatively high for the high-Si boninites and the Mikazukiyama group, and significantly higher than N-MORB (0.02 for Th/Ce, and 0.07 for Th/Nb: Gale et al., 2013), and lower in the Hahajima group (Fig. 5c), comparable or slightly higher than N-MORB. Some of the cpx-opx andesites from the Mikazukiyama group show particularly high Th/Ce and Th/Nb.

Light rare earth element (LREE) ratios such as La/Sm also show differences between the different groups, i.e., the high-Si boninites show the highest La/Sm, higher than N-MORB (1.2: Gale et a., 2013), and the Hahajima Group further extends to the lowest La/Sm ratios among the Bonin Islands volcanics, as low as comparable to N-MORB, while La/Sm ratios in the Mikazukiyama group overlap with those of the high-Si boninites (Fig. 5d).

Middle to heavy rare earth element ratios such as Dy/Yb are lowest in high-Si boninites, and the Hahajima group show the highest ratios, with intermediate ratios for both cpx-opx andesites and low-Si boninites from the Mikazukiyama group (Fig. 5e).

High-Si boninites have lower Sm/Zr than other volcanics from the Bonin Islands and N-MORB (0.034: Gale et al., 2013). Low-Si boninites of the Mikazukiyama group show comparable ratios to the highest ratios amongst the high-Si boninites. The Hahajima group shows decreasing Sm/Zr with increasing Sm, while low-Si boninite and cpx-opx andesite of the Mikazukiyama group have increasing Sm/Zr with increasing Sm (Fig. 5f).

Nb/Zr ratios of Bonin Island volcanics are generally lower than N-MORB (0.036). In the high-Si boninites this ratio is generally 0.012-0.02, with some Mukojima group boninites extending this to 0.035. Most of the low-Si boninites from the Mikazukiyama group have higher Nb/Zr ratios (0.02-0.035) than the high-Si boninites from Chichijima group, and overlap with those of the Hahajima group (Fig. 5g).

Radiogenic isotopes

A clear feature of the Pb isotopes from the Chichijima and Mukojima high-Si boninites are the positive trends extending from $\Delta^{207}Pb/^{204}Pb$ ~2 to 7 and $\Delta^{208}Pb/^{204}Pb$ ~15 to 30, while $^{206}Pb/^{204}Pb$ varies from ~18.5 to 18.7 ($\Delta^{207}Pb/^{204}Pb$ and $\Delta^{208}Pb/^{204}Pb$ are vertical deviation in $^{207}Pb/^{204}Pb$ and $^{208}Pb/^{204}Pb$ from the Northern Hemisphere Reference Line (NHRL: Hart, 1984; Zindler and Hart, 1986), Fig. 6a and b). In $^{207}Pb/^{204}Pb$-$\Delta^{207}Pb/^{204}Pb$ (Fig. 6c), these groups form strong positive correlations extending to high $^{207}Pb/^{204}Pb$ (15.6). In each of these projections, samples from the Mukojima group form a discrete, sub-parallel trend to the Chichijima group, but are offset to ~0.1 higher $^{206}Pb/^{204}Pb$. In contrast, the Mikazukiyama low-Si boninites form a trend extending to high $^{206}Pb/^{204}Pb$ (19.5), low $\Delta^{208}Pb/^{204}Pb$ (-30) and constant $\Delta^{207}Pb/^{204}Pb$ (~-1.5). Mikazukiyama cpx-opx andesites form a short, steep trend close to the NHRL, but with $^{206}Pb/^{204}Pb$ decreasing with increasing ΔPb. This trend is coincident with the upper "off-axis" boninites from IODP Exp. 352 (Fig. 6 a-c). The Hahajima group forms a compact group with similar $^{206}Pb/^{204}Pb$ and $\Delta^{207}Pb/^{204}Pb$ to Pacific MORB, but with $\Delta^{208}Pb/^{204}Pb$ elevated to ~12. Overall, the Hahajima group forms a diffuse trend to lower Δ-values with higher $^{206}Pb/^{204}Pb$, in a similar fashion to the Mikazukiyama low-Si boninites.

High-Si boninites show the highest $^{87}Sr/^{86}Sr$ and lowest $^{143}Nd/^{144}Nd$ ratios among the early arc volcanics from the Bonin Islands. (Fig. 6d). The Hahajima group shows the lowest $^{87}Sr/^{86}Sr$ and highest $^{143}Nd/^{144}Nd$, while cpx-opx andesites and low-Si boninites of the Mikazukiyama group have intermediate ratios between high-Si boninites and the Hahajima group. Figure 6e shows that high-Si boninites from the Chichijima and Mukojima groups have a wide range of $^{143}Nd/^{144}Nd$ (εNd ~2.5-7.5) at constant $^{206}Pb/^{204}Pb$ (18.65 ± 0.1). This compares to Hahajima and Mikazukiyama, which have relatively invariant εNd ~6.5-8.5; regardless of their spread in $^{206}Pb/^{204}Pb$ (18.4-19.5). Despite the spread of εNd on Chichijima there is little corresponding change in εHf (12.1-13.5), which contrasts with Hahajima and Mikazukiyama, where εHf is dispersed in the range 11.3-17.5 (Fig. 6f).

DISCUSSION

Volcanism moves away from the trench

New dating results presented in this study as well as those from IODP Exp. 352 (Reagan *et al.*, 2019) support the earlier interpretations regarding the temporal variation of early arc magmatism (Ishizuka *et al.*, 2006a; 2011a). Following the trench-proximal FAB at 51-52 Ma, magmatism progresses westwards across the arc. Reagan *et al.* (2019) showed that boninites drilled at U1439 of IODP Exp.352 on the trench slope east of the Mukojima Islands are 50.33-51.27 Ma; ~2 Myr older than subaerially-exposed boninites from the Bonin Islands. This result indicates that boninite magmatism started with the low-Si boninite, and then high-Si boninites at around 51 Ma within c. 10 km from the FAB site (Reagan *et al.*, 2019). Subsequently, the location of high-Si boninite magmatism migrated westward, i.e., toward the present day Bonin Islands, and this magmatism lasted around 4 million years until 46 Ma, to be followed by dacite and rhyolite magmatism of the Asahiyama Formation at 45-46 Ma (Table 1, Ishizuka *et al.*, 2006a; 2011a). The Asahiyama volcanics can be viewed as a product of crystal fractionation of boninite magma (Taylor *et al.*, 1994). Ages of the boninites thus imply that the locus of boninite magmatism migrated away from the trench with time.

Low-Si boninite and cpx-opx andesites of the Mikazukiyama group erupted at around 45 Ma, and lasted for less than a million years.

The youngest magmatism (38.4-45 Ma) occurred in the Hahajima group in the southern Bonin Islands, and along the western escarpment of the Bonin Ridge to the west off the Mukojima and Chichijima Islands (Ishizuka *et al.*, 2006a). Furthermore, dredge sampling to the east of Hahajima Island (D30 of KH07-2 cruise; Fig. 1b) recovered boninites, confirming the east-west spatial sequence along this 350 km long segment of the arc. Dating results support for the interpretation that following subduction initiation, magmatism migrated about 80 km away from the trench with time, over a period of 7-8 million years.

Changes in slab input

Isotopic variations amongst the Bonin volcanics could have been generated by a number of potential sources. These are:

1) Pre-existing crust
2) Subducted pelagic or volcaniclastic sediment

3) Subducted igneous ocean crust/lithosphere
4) The supra-subduction mantle (mantle wedge)

These components may contribute to the composition of the system either via a fluid, a melt or as a solid/melted assimilant. In the current Izu-Bonin-Mariana arc, there are good constraints on the isotopic composition and elemental abundances of most of these components (e.g., Hauff *et al.*, 2003; Plank *et al.*, 2007; Durkin *et al., in press*). In general terms at least, the recently subducted and current supra-subduction material are likely to be similar to those of the Eocene. As such, we assume that these compositions can be used to assess inputs to the Bonin Island volcanism. Recent drilling through the Eocene-Oligocene Izu-Bonin-Mariana rear-arc confirmed that pre-existing crust is equivalent to Indian MORB (i.e. Philippine Sea MORB: Hickey-Vargas et al., 1995) ocean crust (Ishizuka *et al.*, 2018; Hickey-Vargas *et al.*, 2018; Yogodzinski *et al.*, 2018). As such, this pre-existing crust has similar Indian isotopic characteristics to the forearc basalts, indicating the mantle wedge was characterised by $\Delta^{208}Pb/^{204}Pb$ ~40 and $\Delta^{207}Pb/^{204}Pb$ 0-3.

Sedimentary components on the current Pacific plate span the age range of Bonin Island volcanism. These comprise pelagic sediments and seamount-derived volcaniclastic sediments, which are variably distributed along the length of the current arc (Kelley *et al.*, 2003; Plank *et al.*, 2007; Straub *et al.*, 2009: Fig. 6). Some latitudinal variation is present in the sedimentary material, for example between ODP Sites 1149 and 801 of the Izu-Bonin and Mariana arcs, respectively (Plank & Langmuir, 1998; Plank *et al.*, 2007: Fig. 6). This may be reflected in the isotopic variation in Pb isotopes along the active Izu-Bonin-Mariana arc (Taylor & Nesbitt, 1998; Ishizuka *et al.*, 2006b, 2007).

Subducted altered ocean crust in the current system is Pacific MORB with seamounts of HIMU or EM composition (Koppers *et al.*, 1998, 2003; Durkin *et al., in press*). It is possible that Indian MORB compositions were present on the Pacific Plate in the Eocene, but have subsequently been consumed by subduction (Straub *et al.*, 2009). Alteration by syn-magmatic hydrothermal processes and by seawater interaction may have modified primary magmatic compositions of volcaniclastic material and oceanic crust. Such processes generally increase U relative to Th and Pb which, as shown in Fig. 6 a-c and e, results in lower $\Delta^{207}Pb/^{204}Pb$ and $\Delta^{208}Pb/^{204}Pb$ (often highly negative) with higher $^{206}Pb/^{204}Pb$ (Hauff *et al.*, 2003; Straub *et al.*, 2009; Li et al., 2019).

Positive correlations between fluid-mobile element enrichment and isotopes, such as Ba and

$^{87}Sr/^{86}Sr$ and $^{206}Pb/^{204}Pb$, are indicative of radiogenic components added to a Indian MORB-type mantle (Fig. 7a). This component has been interpreted as slab-derived material added to the source of boninite magma from the subducting Pacific plate (e.g., Taylor *et al.*, 1994; Ishizuka *et al.*, 2006a, 2011a; Li et al., 2019).

Pb isotope variation within high-Si boninites from the Chichijima and Mukojima groups defines a strong alignment between Pacific pelagic sediment with high ΔPb and Pacific MORB or its altered, subducting equivalent with low ΔPb (Fig. 6a-c). The lack of a trajectory to high $\Delta^{208}Pb/^{204}Pb$ with low $^{206}Pb/^{204}Pb$ excludes significant Pb derived from the Indian MORB mantle wedge ($\Delta^{208}Pb/^{204}Pb > 30$). Notably, Chichijima and Mukojima boninites have Ce/Pb <2 regardless of their Pb isotope ratio (Fig. 7b). This implies that the components that mixed to form the Pb isotope trends must also have similarly low Ce/Pb. Indeed, they have significantly lower Ce/Pb than subducting Pacific crust or Pacific pelagic sediment. This low Ce/Pb is likely a characteristic of fluid released from the subducted crust, which derives its Pb from interaction with variable proportions of MORB and sediment. As this Pb-rich fluid was introduced into an effectively Pb-free depleted mantle wedge, essentially the entire Pb inventory of the resulting partial melts was slab-derived.

Correlations between εNd, $^{206}Pb/^{204}Pb$ and εHf for the high-Si boninites from the Chichijima and Mukojima groups (Fig. 6e, f) are also indicative of pelagic sediment-Pacific MORB interaction. However, the addition of Nd and Hf via subduction implies the carrier may have the characteristics of a melt or supercritical fluid rather than a simple aqueous fluid (e.g., Woodhead *et al.*, 2001). This implication is further supported by a negative correlation between $^{143}Nd/^{144}Nd$ and Th/Ce or La/Sm (Fig. 7c,d).

Taylor *et al.* (1994) proposed that the distinctively low Sm/Zr of Chichijima boninites (0.02 compared to ~0.035 for MORB) resulted from slab melting in the presence of residual amphibole, but not by crystal fractionation of amphibole. This interpretation appears to be applicable to all the high-Si boninites from the Chichijima and Mukojima groups (Fig. 5f). Sm/Zr variation of the Hahajima group, however, seems to be compatible with (cryptic) crystal fractionation of amphibole, as seen in mature volcanic arcs (e.g., Davidson et al., 2007), which consistently explains Sm/Zr variation with Sm content and also decreasing Dy/Yb with increasing SiO_2 (Fig. 5e, f).

After activity of Chichijima and Mukojima high-Si boninite magmatism, volcanism at 44-45 Ma became transitional between boninitic and tholeiitic/calc-alkaline. These eruptives are represented by the low-Si boninites and cpx-opx andesites of the Mikazukiyama group. This switch in magmatism was accompanied by a sharp change in the characteristics of the subduction components. Neither of the Mikazukiyama magma types show any significant indication of a Pb isotope vector towards pelagic sediment. Instead these volcanics trend to negative $\Delta^{208}Pb/^{204}Pb$ and high $^{206}Pb/^{204}Pb$ (18.8 – 19.5) compositions. Other characteristics, such as lower Th/Ce and $^{87}Sr/^{86}Sr$ combined with higher Ce/Pb and $^{143}Nd/^{144}Nd$ (Fig. 6d, 7b,c) are also concordant with a significantly smaller pelagic contribution. The overall implication of this is that, in the central and southern Bonin islands at least, there was a change in the material released from the slab at around 45 Ma. It is also possible that physical conditions in the slab changed at the same time. This, in turn, may change the properties of the slab flux (e.g., hydrous fluid, siliceous melt, supercritical fluid) and consequently influence the trace element concentrations in the slab component (e.g., Kessel *et al.,* 2005).

A possible candidate for a slab-derived component with high $^{206}Pb/^{204}Pb$ and low ΔPb is volcaniclastic material originating from HIMU oceanic islands on the subducting Pacific Plate (Koppers *et al.*, 1998, 2003; Ishizuka *et al.*, 2007). Since HIMU seamounts in the modern Western Pacific are as old as 100-120 Ma (Koppers *et al.*, 2003), it is reasonable to assume that such volcaniclastics were present on the newly subducting Pacific Plate at 45 Ma. Contribution of this volcaniclastic material instead of pelagic sediment is consistent with lower $^{87}Sr/^{86}Sr$ and higher $^{143}Nd/^{144}Nd$ (εNd ~6) in Mikazukiyama compared to the earlier high-Si boninites. Of the two groups within Mikazukiyama, the low-Si boninites have higher Nb/Zr, ΔNb (ΔNb is defined as $\Delta Nb = 1.74 + \log(Nb/Y) - 1.92\log(Zr/Y)$ to express deficiency or excess of Nb relative to the OIB compositions: Fitton et al. (1997)) and $^{206}Pb/^{204}Pb$, suggesting they may have a larger contribution from the HIMU volcaniclastics relative to the cpx-opx andesites (Fig. 8).

A further change in the subduction system occurred with the Hahajima group, which followed the Mikazukiyama group. Hahajima samples shift back to lower $^{206}Pb/^{204}Pb$ (18.5) at $\Delta^{207}Pb/^{204}Pb$ ~0 and higher $^{143}Nd/^{144}Nd$ (εNd ~8), which is consistent with Pacific MORB-type crust in the subduction flux (Fig. 6e). Hahajima is also characterised by a much subdued enrichment in fluid-mobile elements (lowest Ba/Nb, highest Ce/Pb among volcanics from the Bonin Islands: Fig. 5a,b). Given the higher Ce/Pb of Hahajima (5-12), it is possible that a greater proportion of these trace elements were derived from melting of the Indian-MORB-style mantle wedge (Ce/Pb ~25) rather than the subduction fluid (<2). This is also supported by its higher $\Delta^{208}Pb/^{204}Pb$ (~12) and εHf (16), which are transitional between the characteristics of the Indian mantle domain and a subduction input dominated by Pacific MORB (Fig. 6b, f).

Slab derived material can take different physical forms, such as supercritical fluid, siliceous melt or hydrous fluid. The physical properties are chiefly controlled by temperature (e.g., Kawamoto et al., 2012) as well as pressure and source mineral assemblage. Slab-derived material affecting the Quaternary Izu-Bonin frontal arc volcanoes appears to be dominated by hydrous fluid; except its southernmost part around Ioto Island (e.g., Taylor and Nesbitt, 1998; Ishizuka et al., 2007). Hence, a major difference between the earliest Eocene arc and the modern Izu-Bonin arc appears to be that a siliceous melt component was prominent and dominant in early arc relative to the modern arc, whatever the nature of the subducting materials. This might indicate that in the earliest subarc mantle was hotter at a shallower depth relative to the modern arc. Consequently, this allowed the generation of more siliceous melt directly from slab or from reactions between supercritical fluids and the mantle, which released melts with a high-Mg andesitic composition (e.g., Kessel et al., 2005; Mibe et al., 2011; Kawamoto et al., 2012).

Nature of the subducting slab

Bonin Islands magmatism describes the evolution of a nascent arc and indicates that there were a series of distinct changes in the subduction flux within a period of 4 million years (Fig. 9a-c). Following the Indian MORB-like forearc basalts, the initial high-Si boninite arc magmas at ~48 Ma reflect a flux of melt or supercritical fluid derived from subducted crust comprising accumulations of pelagic sediment on Pacific MORB (Fig. 9a, d).

Following this at 45 Ma, the slab flux briefly switched to originating from a combination of HIMU-style sediment and Pacific MORB, before Pacific-MORB became the dominant subduction input to the mantle wedge at ~44 Ma. A transient HIMU signature such as this is compatible with a 30 km diameter seamount subducted at 4 cm/year, which would take < 1 Myr to pass beneath the arc (Fig. 9b, d). This estimate is consistent with the short duration of Mikazukiyama group activity with a strong signature of ocean island volcano-derived material. After the seamount passed, it appears that the Pacific plate provided a negligible amount of sediment, because the Hahajima group are dominated by a signature of Pacific ocean crust (Fig. 9c, d). This lack of pelagic sediment after 45 Ma might be explained by the following scenarios: 1) pelagic sediment was absent from areas of the subducting plate e.g. on young ocean crust or in an environment not suitable for pelagic sedimentation. 2) Pelagic sediment was not subducted because it was scraped off and accreted to the trench slope. 3) Subducting pelagic sediment released its melt or fluid flux before it reached the melt generation depth for Hahajima.

Assuming that the Pacific plate was being subducted, a drastic change in the age of the crust seems unlikely, except in the presence of hotspot-related seamounts. Variation of the CCD could cause a variation in sediment thickness and composition via the abundance of biogenic carbonate. Sedimentary carbonate could cause a dilution of all trace elements except Sr (and Sr is not highly enriched in currently subducting Izu-Bonin carbonate sediment; Plank et al., 2007). This implies that carbonate variation in the subducting sediment probably does not significantly change the isotopic composition (at least for Nd and Pb) of subducting sediment. Siliceous biogenic sediment can also dilute the enrichment of continentally-derived pelagic clays and/or sediments, hence should not affect the isotopic and trace element signature of subducting sediment.

Based on recent plate reconstruction models, the location of subduction nucleation for the Izu-Bonin arc is predicted to have been far from continents (Seton et al., 2015: Wu et al., 2016). Eurasia is the most likely source of terrigenous sediment, but its contribution is expected to have been relatively small, and has not changed significantly in this time period. Accordingly, it is hard to explain the lack of a sediment signature simply via compositional variation of the subducting sediment: an absence of pelagic sediment seems more likely.

An extensional stress regime on the overriding plate (i.e., the Philippine Sea plate) generated spreading and FAB magmatism during the initial stages of subduction. This extension appears to have prevailed until the end of boninite magmatism at around 45 Ma (Umino, 1985; Umino & Nakano, 2007). After 45 Ma, there is little evidence for the development of a parallel dyke swarm. This implies a change in regional stress regime, i.e., a decreasing differential stress between $\sigma1$ and $\sigma3$ in the horizontal plane, indicating a cessation of regional extension. This change in the stress regime might have been linked to trench retreat and/or a variation in the rate of convergence. In turn, these could potentially affect the rate of erosion or accretion at the trench (e.g., Clift & Vannucchi, 2004) and hence align with the second scenario above. Lower crust and upper mantle are exposed along the Izu-Ogasawara Trench (Ishizuka et al., 2011; Morishita et al., 2011), which implies that erosion or extension in the forearc has uncovered the deepest arc. The timing of this exposure is not clear, but this implies that the Izu-Ogasawara trench was erosional at some point after boninite magmatism, and the accreted sediment, if any, could have been removed at any time between the Eocene and present.

In terms of the third scenario, some evidence for dehydration of the slab in the forearc can be taken from the occurrence of serpentinite derived from mantle harzburgite found in the Izu forearc at ODP Sites 783 and 784 (Fryer et al., 1990: Ishii et al., 1992). Kamimura et al. (2002) obtained a seismic velocity structure of the Izu forearc including the serpentinite-based Torishima Seamount. They proposed that the low velocity in the forearc mantle corresponded to serpentinised peridotite hydrated by dehydration of the subducting slab. Serpentinisation of the forearc mantle is expected to occur below 600^{o}C, and hence be amagmatic (e.g., Hyndman and Peacock, 2003; Ribeiro et al., 2019). Accordingly, even though the age of the serpentinisation is not clear, sediment dehydration in the forearc without magmatism is a possibility after 45 Ma.

The locus of magmatism appears to have migrated by about 80 km within 5 million years from near the trench to the Bonin Islands. This does not simply mean that a specific point of the subducting slab moved this distance away from the trench as slab flux clearly changed with time. However, if we assume a subduction angle of 45^{o} and a minimum subduction rate of around 3-4 cm/year, this could explain the migration of volcanic activity. The slab depth is expected to be greater than 40 km, based on the depth estimate for melt extraction of boninites at 48 Ma (by assuming that melt extraction occurred in the mantle wedge: Umino *et al.*, 2015), which is consistent with the above estimate for the rate of subduction.

Since the locus of Eocene magmatism migrated away from the trench, the chemical composition of magmatism is likely to have been influenced by a progressively deeper release from the slab. At this time the mantle also was free of earlier metasomatism, i.e. the subduction flux was added to a "clean sheet" mantle source. Combining the progressive deepening and the initially flux-free mantle may explain why the nascent arc records sharp changes in the slab flux compared to the modern mature arc.

CONCLUSION

High-precision isotope data combined with $^{40}Ar/^{39}Ar$ dating constrain the chemical evolution of the Izu-Bonin system as it responded to the initiation of subduction. Volcanic activity migrated 80 km away from the trench over a period of 5 million years, in response to the progressive descent of the slab until the establishment of steady-state subduction.

1) Following initial spreading and MORB-like magmatism (50-52 Ma), and short period of

activity of low-Si boninite near axis at 51 Ma, the nascent arc erupted high-Si boninite adjacent to the trench (46-50 Ma). This progressed into low-Si boninite and cpx-opx andesites (45 Ma), then tholeiitic and calcalkaline magmatism (38.4-45 Ma).

2) These changes in magma type coincided with sharp changes in the slab-derived flux. On the Bonin Islands, initial high-Si boninites reflect a pelagic sediment and MORB-derived flux. This was replaced by a HIMU-type volcaniclastic signature in the following low-Si boninites. In turn, this signature was replaced by a Pacific MORB-dominated flux in the post 45 Ma volcanics.
3) Trace element data suggest that the flux-free mantle wedge composition was initially a harzburgitic, potentially residual following forearc basalt removal. At 45 Ma this changed to a less depleted mantle with characteristics similar to Philippine Sea MORB source.
4) Changes in slab-flux and mantle wedge composition may be a response to the unique and transient conditions following subduction initiation. Subduction-free mantle in the nascent arc allowed preservation of a clear time-record of the changing subducted material. In maturity, the arc tapped an upwelling asthenosphere that was imparted with an integrated average flux reflecting a combination of the sedimentary and ocean crust components.

ACKNOWLEDGEMENTS

We would like to thank K. Yamanobe for preparation of glass beads and assistance with the ICP-MS measurements. We appreciate A. Owada, T. Sato and E. Hirabayashi for preparation of thin sections. We also thank T. Sasaki, T. Shimono, A. Tokumoto, and H. Nagato for helping preparation of rock powder, and N. Geshi and Y. Ishizuka for the maintenance of GSJ XRF laboratory. Andy Milton and Agnes Michalik are thanked for assistance in the Southampton isotope laboratories. We appreciate IMR, Tohoku University and Oregon State University for neutron irradiation. This work was supported by Grant-in-Aid (B) (No. 25287133), (C) (No. 17K05686) and JSPS bilateral grant (Japan-UK) for OI. The authors acknowledge the constructive reviews by anonymous reviewers and helpful editorial comments by Georg Zellmer and Marjorie Wilson.

SUPPLEMENTARY DATA

Supplementary data are available at Journal of Petrology online.

REFERENCES

Blichert-Toft, J. & Albarede, F. (1997). The Lu-Hf isotope geochemistry of chondrites and the evolution of the mantle-crust system. *Earth and Planetary Science Letters* **148**, 243–258.

Chauvel, C., Marini, J.-C., Plank, T. & Ludden, J. (2009). Hf-Nd input flux in the Izu-Mariana subduction zone and recycling of subducted material in the mantle. *Geochemistry Geophysics Geosystems* **10**, 2008GC002101.

Chu, N. C., Taylor, R. N., Chavagnac, V., Nesbitt, R. W., Boella, R. M., Milton, J. A., German, C. R., Bayon, C. & Burton, K. (2002). Hf isotope ratio analysis using multi-collector inductively coupled plasma mass spectrometry: an evaluation of isobaric interference corrections. *Journal of Analytical Atomic Spectrometry* **17**, 1567–1574.

Clift, P. & Vannucchi, P. (2004). Controls on tectonic accretion versus erosion in subduction zones: Implications for the origin and recycling of the continental crust. *Reviews of Geophysics* **42**, RG2001, doi:10.1029/2003RG000127.

Cosca, M. A., Arculus, R. J., Pearce, J. A. & Mitchell, J.G. (1998). $^{40}Ar/^{39}Ar$ and K-Ar geochronological age constraints for the inception and early evolution of the Izu-Bonin-Mariana arc system. *The Island Arc* **7**, 579-595.

Davidson, J. P., Turner, S., Handley, H., Macpherson, C. & Dosseto, A. (2007). An amphibole 'sponge' in arc crust? *Geology* **35**, 787-790.

Durkin, K., Castillo, P. R., Straub, S. M., Abe, N., Tamura, Y. & Yan, Q. (in press). An origin of the along-arc compositional variation in the Izu-Bonin arc system. *Geoscience Frontiers* doi.org/10.1016/j.gsf.2019.12.004.

Fitton, J. G., Saunders, A. D., Norry, M. J., Hardarson, B. S. & Taylor, R.N. (1997). Thermal and chemical structure of the Iceland plume. *Earth and Planetary Science Letters* **153**, 197–208.

Fleck, R.J., Sutter, J.F. & Elliot, D.H. (1977). Interpretation of discordant $^{40}Ar/^{39}Ar$ age-spectra of Mesozoic tholeiites from Antarctica. *Geochimica et Cosmochimica Acta* **41**, 15-32.

Fryer, P., Pearce, J. A., Stokking, L. B., et al. (1990). *Proceedings of the Ocean Drilling Program Initial Reports*: Ocean Drilling Program, College Station, TX, **125.**

Gale A., Dalton, C. A., Langmuir, C. H., Su, Y. & Schilling, J.-G. (2013). The mean composition of ocean ridge basalts. *Geochemistry Geophysics Geosystems* **14**, doi:10.1029/2012GC004334.

Hall, C.E., Gurnis, M., Sdrolias, M., Lavier, L.L. & Muellar, R.D. (2003). Catastrophic initiation of subduction following forced convergence across fracture zones. *Earth and*

Planetary Science Letters **212**, 15-30.

Hart, S. R. (1984). A large-scale isotopic anomaly in the Southern hemisphere mantle. *Nature* **309**, 753–757.

Hauff, F., Hoernle, K. & Schmidt, A. (2003). Sr–Nd–Pb composition of Mesozoic Pacific oceanic crust (Site 1149 and 801, ODP Leg 185): implications for alteration of ocean crust and the input into the Izu-Bonin-Mariana subduction system. *Geochemistry Geophysics Geosystems* **4(8)**,8913, doi:10.1029/2002GC000421.

Hickey-Vargas, R. (1991). Isotope characteristics of submarine lavas from the Philippine Sea: implications for the origin of arc and basin magmas of the Philippine tectonic plate. *Earth and Planetary Science Letters* **107**, 290-304.

Hickey-Vargas, R., Hergt, J. M. & Spadea, P. (1995). The Indian Ocean-type isotopic signature in Western Pacific marginal basins. In: Taylor B. & Natland, J. (eds) *Origin and significance in Active Margins and Marginal Basins of the Western Pacific*. *American Geophysical Union, Geophysical Monograph* **88**, 175-197.

Hickey-Vargas, R. (1998). Origin of the Indian Ocean-type isotopic signature in basalts from Philippine Sea Plate spreading centers: An assessment of local versus large-scale processes. *Journal of Geophysical Research* **103**, 20963-20979.

Hickey-Vargas, R., Yogodzinski, G. M., Ishizuka, O., McCarthy, A., Bizimis, M., Kusano, Y., Savov, I. P. & Arculus, R. (2018). Origin of depleted basalts during subduction initiation and early development of the Izu-Bonin-Mariana Island arc: Evidence from IODP Expedition 351 Site U1438, Amami-Sankaku Basin. *Geochimica et Cosmochimica Acta* **229**, 85–111.

Hyndman, R. D. & Peacock, S. M. (2003). Serpentinization of the forearc mantle. *Earth and Planetary Science Letters* **212**, 417-432.

Ishii, T., Robinson, P. T., Maekawa, H. & Fiske, R. (1992). Petrological studies of peridotites from diapiric serpentinite seamounts in the Izu-Ogasawara–Mariana forearc, Leg 125. *Proceedings of the Ocean Drilling Program Scientific Results* **125**, 445–485.

Ishizuka, O., Taylor, R. N., Milton, J. A. & Nesbitt, R. W. (2003). Fluid-mantle interaction in an intra-oceanic arc: constraints from high-precision Pb isotopes. *Earth and Planetary Science Letters* **211**, 221-236.

Ishizuka, O., Kimura, J., Li, Y., Stern, R., Reagan, M., Taylor, R., Ohara, Y., Bloomer, S., Ishii, T. & Hargrove III, U. (2006a). Early stages in the evolution of Izu–Bonin arc volcanism: new age, chemical, and isotopic constraints. *Earth and Planetary Science Letters* **250**, 385-401.

Ishizuka, O., Taylor, R. N., Milton J. A., Nesbitt, R. W., Yuasa, M. & Sakamoto, I. (2006b). Variation in the source mantle of the northern Izu arc with time and space -Constraints from high-precision Pb isotopes -. *Journal of Volcanology and Geothermal Research* **156**, 266-290.

Ishizuka, O., Taylor, R. N., Milton J. A., Nesbitt, R. W., Yuasa, M. & Sakamoto, I. (2007). Processes controlling along-arc isotopic variation of the southern Izu-Bonin arc. *Geochemistry Geophysics Geosystems* **8**, Q06008, doi:10.1029/2006GC001475.

Ishizuka, O., Yuasa, M., Taylor, R. N. & Sakamoto, I. (2009). Two contrasting magmatic types coexist after the cessation of back-arc spreading. *Chemical Geology* **266**, 283-305.

Ishizuka, O., Yuasa, M., Tamura, Y., Shukuno, H., Stern, R. J., Naka, J., Joshima, M. & Taylor, R. N. (2010). Migrating shoshonitic magmatism tracks Izu-Bonin-Mariana intra-oceanic arc rift propagation. *Earth and Planetary Science Letters* **294**, 111-122.

Ishizuka, O., Tani, K., Reagan, M. K., Kanayama, K., Umino, S., Harigane, Y., Sakamoto, I., Miyajima, Y., Yuasa, M. & Dunkley, D.J. (2011a). The timescales of subduction initiation and subsequent evolution of an oceanic island arc. *Earth and Planetary Science Letters* **306**, 229-240.

Ishizuka, O., Taylor, R. N., Yuasa, M. & Ohara, Y. (2011b). Making and breaking an Island arc: a new perspective from the Oligocene Kyushu-Palau arc, Philippine Sea. *Geochemistry Geophysics Geosystems* **12**, Q05005, doi:10.1029/2010GC003440.

Ishizuka, O., Taylor, R. N., Ohara, Y. & Yuasa, M. (2013). Upwelling, rifting and age-progressive magmatism from the Oki-Daito mantle plume. *Geology* **41**, 1011-1014.

Ishizuka, O., Tani, K. & Reagan, M. K. (2014a). Izu-Bonin-Mariana fore-arc crust as a modern ophiolite analogue. *Elements* **10**, 115-120.

Ishizuka, O., Umino, S., Taylor, R. N. & Kanayama, K. (2014b). Evidence for hydrothermal activity in the earliest stages of intraoceanic arc formation: implication to ophiolite-hosted hydrothermal activity. *Economic Geology* **109**, 2159-2177.

Ishizuka, O., Hickey-Vargas, R., Arculus, R. J., Yogodzinski, G. M., Savov, I. P., Kusano, Y., McCarthy, A., Brandl, P. & Sudo, M. (2018). Age of Izu-Bonin-Mariana arc basement. *Earth and Planetary Science Letters* **481**, 80-90.

Johnson, C. M. & Beard, B. L. (1999). Correction of instrumentally produced mass fractionation during isotopic analysis of Fe by thermal ionization mass spectrometry. *International Journal of Mass Spectrometry* **193**, 87-99.

Kamimura, A., Kasahara, J., Shinohara, M., Hino, R., Shiobara, H., Fujie, G. & Kanazawa, T.

812 (2002). Crustal structure study at the Izu-Bonin subduction zone around 31°N: implications of serpentinized materials along the subduction plate boundary. *Physics of the Earth and Planetary Interiors* **132**, 105–129, doi:10.1016/S0031-9201(02)00047-X.

815 Kanayama, K., Umino, S. & Ishizuka, O. (2012). Eocene volcanism during the incipient stage of Izu–Ogasawara Arc: Geology and petrology of the Mukojima Island Group, the Ogasawara Islands. *The Island Arc* **21**, 288–316.

818 Kanayama, K., Umino, S. & Ishizuka, O. (2014). Shallow submarine volcano group in the early stage of island arc development: Geology and petrology of small islands south off Hahajima main island, the Ogasawara Islands. J*ournal of Asian Earth Sciences* **85**, 1–25.

821 Kawamoto, T., Kanzaki, M., Mibe, K., Matsukage, K. N. & Ono, S. (2012). Separation of supercritical slab-fluids to form aqueous fluid and melt components in subduction zone magmatism. *Proceedings of the National Academy of Sciences of the United States of America* **109**, 18695–18700.

825 Kelley, K. A., Plank, T., Ludden, J. & Staudigel, H. (2003). Composition of altered oceanic crust at ODP Sites801 and 1149. *Geochemistry Geophysics Geosystems* **4**(6), doi:10.1029/2002GC000435.

828 Kessel, R., Schmidt, M. W., Ulmer, P. & Pettke, T. (2005). Trace element signature of subduction-zone fluids, melts and supercritical liquids at 120-180km depth. *Nature* **437**(29), 724-727.

831 Koppers, A. A. P., Staudigel, H., Wijbrans, J. R. & Pringle, M. S. (1998). The Magellan seamount trail: implications for Cretaceous hotspot volcanism and absolute Pacific plate motion. *Earth and Planetary Science Letters* **163**, 53-68.

834 Koppers, A. A. P., Staudigel, H., Pringle, M. S. & Wijbrans, J. R. (2003). Short-lived and discontinuous intraplate volcanism in the South Pacific: Hot spots or extensional volcanism? *Geochemistry Geophysics Geosystems* **4**(10), doi:10.1029/2003GC000533.

837 Li, H. -Y., Taylor, R. N., Prytulak, J., Kirchenbaur, M., Shervais, J. W., Ryan, J. G., Godard, M., Reagan, M. & Pearce, J. A. (2019). Radiogenic isotopes document the start of subduction in the Western Pacific. *Earth and Planetary Science Letters* **518**, 197–210.

840 Li, Y. -B., Kimura, J. -I., Machida, S., Ishii, T., Ishiwatari, S., Maruyama, S., Qiu, N.-N., Ishikawa, T., Kato, Y., Haraguchi, S., Takahata, N., Hirahara, Y. & Miyazaki, T. (2013). High-Mg adakite and low-Ca boninite from a Bonin fore-arc seamount: implications for the reaction between slab melts and depleted mantle. *Journal of Petrology* **54**, 1149-1175.

844 Mibe, K., Kawamoto, T., Matsukage, K. N., Fei, Y. & Ono, S. (2011) Slab melting versus slab

dehydration in subduction-zone magmatism. *Proceedings of the National Academy of Sciences of the United States of America* **1088**, 177–8182.

Miyashiro, A. (1974). Volcanic rock series in island arcs and active continental margins. *American Journal of Science* **257**, 609-647.

Miyazaki, T., Kimura, J.-I., Senda, R., Bogdan, V., Chang, Q., Takahashi, T., Hirahara, Y., Hauff, F., Hayasaka, Y., Sano, S., Shimoda, G., Ishizuka, O., Kawabata, H., Hirano, N., Machida, S., Ishii, T., Tani, K. & Yoshida, T. (2015). Missing western half of the Pacific Plate: Geochemical nature of the Izanagi-Pacific Ridge interaction with a stationary boundary between the Indian and Pacific mantles. *Geochemistry, Geophysics, Geosystems* **16**, 3309-3332.

Plank, T. & Langmuir, C. H. (1998). The chemical composition of subducting sediment and its consequences for the crust and mantle. *Chemical Geology* **145**, 325-394.

Plank, T., Kelley, K. A., Murray, R. W. & Stern, L. Q. (2007). Chemical composition of sediments subducting at the Izu-Bonin trench. *Geochemistry, Geophysics, Geosystems* **8**, Q04I16, doi:10.1029/2006GC001444.

Reagan, M. K., Ishizuka, O., Stern, R. J., Kelley, K. A., Ohara, Y., Blichert-Toft J., Bloomer, S. H., Cash, J., Fryer, P., Hanan, B. B., Hickey-Vargas, R., Ishii, T., Kimura, J. I., Peate, D. W., Rowe, M. C. & Woods, M. (2010). Fore-arc basalts and subduction initiation in the Izu-Bonin-Mariana system. *Geochemistry, Geophysics, Geosystems* **11**, Q03X12, doi:10.1029/2009GC002871.

Reagan, M. K., Pearce, J. A., Petronotis, K., Almeev, R. R., Avery, A. J., Carvallo, C., Chapman, T., Christeson, G. L., Ferré, E. C., Godard, M., Heaton, D. E., Kirchenbaur, M., Kurz, W., Kutterolf, S., Li, H., Michibayashi, K., Morgan, S., Nelson, W. R., Prytulak, J., Python, M., Robertson, A. H. F., Ryan, J. G., Sager, W. W., Sakuyama, T., Shervais, J. W., Shimizu, K. & Whattam, S.A. (2017). Subduction initiation and ophiolite crust: new insights from IODP drilling. *International Geology Review* **59**, DOI: 10.1080/00206814.2016.1276482.

Reagan, M. K., Heaton, D. E., Schmitz, M. D., Pearce, J. A., Shervais, J. W. & Koppers, A. A. P. (2019). Forearc ages reveal extensive shortlived and rapid seafloor spreading following subduction initiation. *Earth and Planetary Science Letters* **506**, 520–529.

Ribeiro, J., Ishizuka, O., Lee, C-T. A. & Girard, G. (2019). Evolution and maturation of the nascent Mariana arc. *Earth and Planetary Science Letters* **530**, https://doi.org/10.1016/j.epsl.2019.115912.

Savov, I. P., Hickey-Vargas, R., D'Antonio, M., Ryan, J. G. & Spadea, P. (2006). Petrology and geochemistry of West Philippine Basin basalts and early Palau-Kyushu arc volcanic clasts from ODP Leg 195, Site 1201D: Implications for the early history of the Izu-Bonin-Mariana Arc. *Journal of Petrology* **47**, 277-299.

Seton, M., Flament, N., Whittaker, J., Müller, R. D., Gurnis, M. & Bower, D. J. (2015). Ridge subduction sparked reorganization of the Pacific plate-mantle system 60–50 million years ago. *Geophysical Research Letters* **42**, 1732–1740.

Shervais, J. W., Reagan, M., Haugen, E., Almeev, R. R., Pearce, J. A., Prytulak, J., Ryan, J. G., Whattam, S. A., Godard, M., Chapman, T., Li, H., Kurz, W., Nelson, W., Heaton, D., Kirchenbaur, M., Shimizu, K., Sakuyama, T., Li, Y. & Vetter, S. K. (2019). Magmatic response to subduction initiation: Part 1. Fore-arc basalts of the Izu-Bonin arc from IODP Expedition 352. *Geochemistry, Geophysics, Geosystems* **20**, https://doi.org/10.1029/2018GC007731.

Steiger, R. H. & Jäger, E. (1977). Subcommision on Geochronology: convention on the use of decay constants in geo- and cosmochronology. *Earth and Planetary Science Letters* **36**, 359-362.

Stern, R. J. & Bloomer, S. H. (1992). Subduction zone infancy: examples from the Eocene Izu-Bonin-Mariana and Jurassic California Arcs. *Geological Society of America Bulletin* **104**, 1621-1636.

Stern, R. J. (2004). Subduction Initiation: Spontaneous and Induced. *Earth and Planetary Science Letters* **226**, 275-292.

Stern, R. J., Reagan, M., Ishizuka, O., Ohara, Y. & Whattam, S. (2012). To understand subduction initiation, study forearc crust; to understand forearc crust, study ophiolites. *Lithosphere* **4**, 469–483.

Straub, S. M., Goldstein, S. L., Class, C. & Schmidt, A. (2009). Mid-ocean-ridge basalt of Indian type in the northwest Pacific Ocean basin. *Nature Geoscience* **2**, 286-289.

Straub, S. M., Woodhead, J. D. & Arculus, R. J. (2015). Temporal evolution of the Mariana Arc: mantle wedge and subducted slab controls revealed with a tephra perspective. *Journal of Petrology* **56**, 409–439.

Tanaka, T., Togashi, S., Kamioka, H., Amakawa, H., Kagami, H., Hamamoto, T., Yuhara, M., Orihashi, Y., Yoneda, S., Shimizu, H., Kunimaru, T., Takahashi, K., Yanagi. T., Nakano, T., Fujimaki, H., Shinjo, R., Asahara. Y., Tanimizu, M. & Dragusanu, C. (2000). JNdi-1: a neodymium isotopic reference in consistency with LaJolla neodymium. *Chemical Geology* **168**, 279-281.

Taylor, B. (1992). Rifting and the volcanic-tectonic evolution of the Izu-Bonin-Mariana Arc. In: Taylor B. & Fujioka K. et al., (eds) *Proceedings of the Ocean Drilling Program, Scientific Results* **126**, 627-651.

Taylor, R. N., Nesbitt, R. W., Vidal, P., Harmon, R. S., Auvray, B. & Croudace, I. W. (1994). Mineralogy, chemistry, and genesis of the Boninite Series Volcanics, Chichijima, Bonin Islands, Japan. *Journal of Petrology* **35**, 577-617.

Taylor, R. N. & Nesbitt, R. W. (1995). Arc volcanism in an extensional regime at the initiation of subduction: A geochemical study of Hahajima, Bonin Islands, Japan. In: Smellie, J. (ed) *Volcanism associated with Extension at Consuming Plate Margins.* Geological Society, London, Special Publications **81**, 115-134.

Taylor, R. N. & Nesbitt, R. W. (1998). Isotopic characteristics of subduction fluids in an intra-oceanic setting, Izu-Bonin Arc, Japan. *Earth and Planetary Science Letters* **164**, 79-98.

Taylor, R. N., Ishizuka, O., Michalik, A., Milton, J. A. & Croudace, I. W. (2015). Evaluating the precision of Pb isotope measurement by mass spectrometry. *Journal of Analytical Atomic Spectrometry* **30**, 198-213.

Thirlwall, M. E. (1991). Long-term reproducibility of multicollector Sr and Nd isotope ratio analysis. *Chemical Geology (Isotope Geoscience Section)* **94**, 85-104.

Uchiumi, S. & Shibata, K. (1980). Errors in K-Ar age determination. *Bulletin of Geological Survey of Japan* **31**, 267-273 (in Japanese with English abstract).

Umino, S. (1985). Volcanic geology of Chichijima, the Bonin Islands (Ogasawara Islands). *The Journal of the Geological Society of Japan* **91**, 505-523.

Umino, S. & Nakano, S. (2007). *Geology of the Chichijima Retto District*. Quadrangle Series, 1:50000, Geological Survey of Japan, AIST, 63p (in Japanese with English abstract).

Umino, S., Nakano, S., Ishizuka, O. & Komazawa, M. (2009). *Geological Map of Japan 1:200,000, Ogasawara Shoto* (in Japanese). Geological Survey of Japan, AIST.

Umino, S., Kitamura, K., Kanayama, K., Tamura, A., Sakamoto, N., Ishizuka, O. & Arai, S. (2015). Thermal and chemical evolution of the subarc mantle revealed by spinel-hosted melt inclusions in boninite from the Ogasawara (Bonin) Archipelago. *Geology* **43**, 151-154.

Umino, S., Ishizuka, O. & Kanayama, K. (2016). *Geology of the Hahajima Retto district*. Quadrangle Series, 1:50000, Geological Survey of Japan, AIST, 46p (in Japanese with English abstract).

Umino, S., Kanayama, K., Kitamura, K., Tamura, A., Ishizuka, O., Senda, R. & Arai, S. (2018). Did boninite originate from the heterogeneous mantle with recycled ancient slab?*Island Arc* **27**, e12221, doi: 10.1111/iar.12221.

Willbold, M. & Stracke, A. (2006). Trace element composition of mantle end-members: Implications for recycling of oceanic and upper and lower continental crust, *Geochemistry Geophysics Geosystems* **7**, Q04004, doi:10.1029/2005GC001005.

Woodhead J., Hergt J., Davidson J. P. & Eggins S. M. (2001). Hafnium isotope evidence for 'conservative' element mobility during subduction zone processes. *Earth and Planetary Science Letters* **192**, 331–346.

Wu, J., Suppe, J., Lu, R. & Kanda, R. (2016). Philippine Sea and East Asian plate tectonics since 52 Ma constrained by new subducted slab reconstruction methods. *Journal of Geophysical Research***121**, 4670–4741.

Yogodzinski, G., Bizimis, M., Hickey-Vargas, R., McCarthy, A., Hocking, B. D., Savov, I. P., Ishizuka, O. & Arculus, R. (2018). Implications of Eocene-age Philippine Sea and Forearc basalts for initiation and early history of the Izu-Bonin-Mariana arc. *Geochimica et Cosmochimica Acta* **228**, 136-156.

York, D. (1969). Least squares fitting of a straight line with correlated errors. *Earth and Planetary Science Letters* **5**, 320-324.

Zindler, A. & Hart, S. (1986). Chemical geodynamics. *Annual Review of Earth and Planetary Sciences***14**, 493-571.

Figure captions

Fig. 1. a) Overview of the bathymetry of the Izu-Bonin-Mariana arc and location of the Bonin Ridge, b) Location of the Bonin Islands with bathymetric map of the Bonin Ridge. Locations of studied islands and submarine sampling stations are shown with the symbols used in the geochemical plots. (Ishizuka *et al.*, 2006a, 2011a; Reagan *et al.*, 2017). Fig. 1a and 1b are modified from Ishizuka *et al.* (2011a). Distribution of each rock type is indicated by the black dashed lines.

Fig. 2. Schematic stratigraphic section and overall chemostratigraphic variation through the Bonin Ridge forearc crust. Rock types and symbols shown in this figure remain consistent through the geochemical plots in all figures. Average content of SiO_2, CaO and TiO_2 projected to 8% MgO (Si8, Ca8 and Ti8) for each stratigraphic unit are shown in the columns to the right.

Fig. 3. $^{40}Ar/^{39}Ar$ age spectra and Ca/K plots for groundmass samples from the Bonin Islands.

Fig. 4. Major element composition of volcanic rocks from the Bonin Islands. Variation of SiO_2 with a) MgO, b) FeO*(FeO^{total})/MgO (Line distinguishing the tholeiitic and calc-alkaline field is from Miyashiro (1974)), and variation of MgO with c) TiO_2, and d) CaO. Data of boninites from IODP Exp. 352 are from Li *et al.* (2019).

Fig. 5. Incompatible trace element ratios for the Bonin Islands. Variation of a) Ce/Pb, b) Ba/Nb, c) Th/Ce, d) La/Sm, e) Dy/Yb with SiO_2 in wt%, f) Sm/Zr with Sm in ppm and g) Nb/Zr with MgO in wt%. Data of boninites from IODP Exp. 352 are from Li *et al.* (2019). Symbols as in Fig. 4. Average trace element ratios for all normal MORB (Gale et al., 2013) are shown. Dashed line with arrow in each plot (where the partition coefficient data is available) qualitatively show effect of fractionation of amphibole as a guide based on partition coefficients for basalt and andesite compiled in the GERM data base (https://earthref.org).

Fig. 6. Radiogenic isotope variation for the Bonin Islands plotted with potential slab and mantle components. a) $\Delta^{207}Pb/^{204}Pb$ vs. $^{206}Pb/^{204}Pb$, b) $\Delta^{208}Pb/^{204}Pb$ vs. $^{206}Pb/^{204}Pb$, c) $\Delta^{207}Pb/^{204}Pb$ vs. $^{207}Pb/^{204}Pb$, d) εNd vs. $^{87}Sr/^{86}Sr$, e) εNd vs. $^{206}Pb/^{204}Pb$, f) εHf vs. εNd. Assumed compositions of subducting igneous crust and sediment are shown (Table S7). Pelagic sediment outboard of Izu-Bonin arc: Plank *et al.* (2007), Pelagic sediment outboard of Mariana arc: Plank & Langmuir (1998), Subducting altered igneous Pacific crust: Hauff *et al.* (2003), volcaniclastic sediment derived from HIMU oceanic islands: Plank & Langmuir (1998). Philippine Sea MORB: Hickey-Vargas (1991, 1998), Savov *et al.* (2006), Ishizuka *et al.* (2009, 2010, 2011b, 2013). Pacific MORB data was compiled from the Earthchem data base

(https://www.earthchem.org). Least squares regression lines are shown in Pb isotopic plots for some rock types with sufficient data. Symbols are as on Fig. 4. Isotopic ratios plotted in these figures are not age-corrected.

Fig. 7. Isotope versus trace element ratio plots for the Bonin Islands volcanics. Data sources are the same as for Figure 6. Least squares regression lines are shown in panel b. Symbols as in Fig. 4.

Fig. 8. Nb/Zr vs. $^{206}Pb/^{204}Pb$ plot. A vector towards volcaniclastic sediment derived from HIMU oceanic islands is shown (Plank & Langmuir, 1998). Symbols as in Fig. 4.

Fig. 9. Schematic diagram showing the progressive variation in the nature of the slab flux following subduction initiation. a) Chichijima/Mukojima group, 48-45 Ma: shallow melting (~35 km) with flux from pelagic sediment and Pacific Ocean igneous crust added to a harzburgitic mantle; b) Mikazukiyama group, 45-44 Ma: melting at ~35 km, slightly further from the trench, flux from HIMU volcaniclastic sediment added to a less depleted mantle source; c) Hahajima group, <45 Ma: deeper melting (~60 km) further from the trench with flux from Pacific Ocean crust added to an upwelling, more fertile mantle source. d) Schematic diagram showing the estimated scale and duration of flux components on the subducting slab.

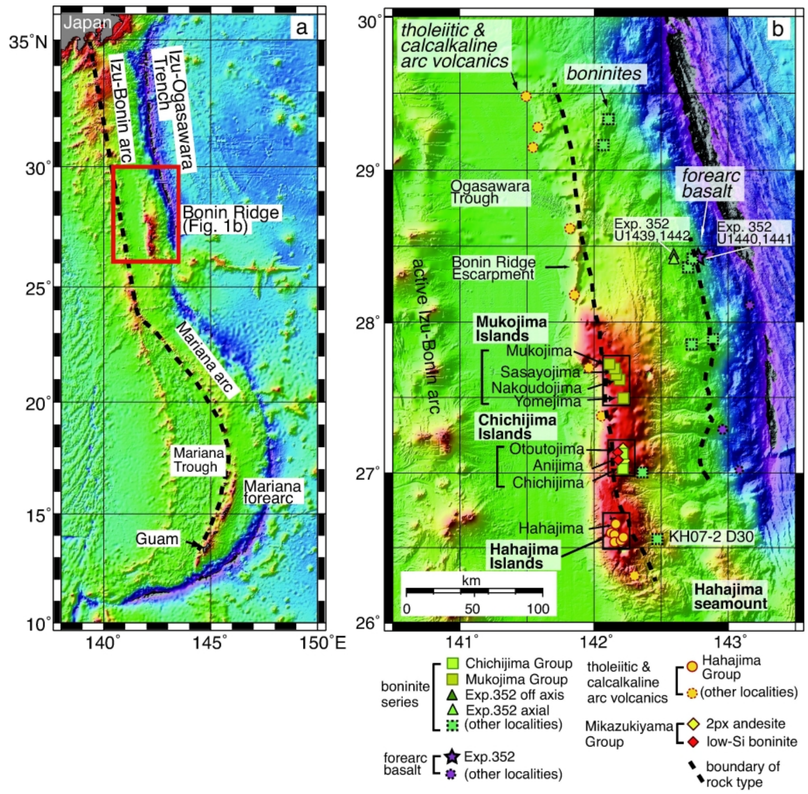

Fig. 1 Ishizuka et al.

Fig. 1. a) Overview of the bathymetry of the Izu-Bonin-Mariana arc and location of the Bonin Ridge, b) Location of the Bonin Islands with bathymetric map of the Bonin Ridge. Locations of studied islands and submarine sampling stations are shown with the symbols used in the geochemical plots. (Ishizuka et al., 2006a, 2011a; Reagan et al., 2017). Fig. 1a and 1b are modified from Ishizuka et al. (2011a). Distribution of each rock type is indicated by the black dashed lines.

146x211mm (600 x 600 DPI)

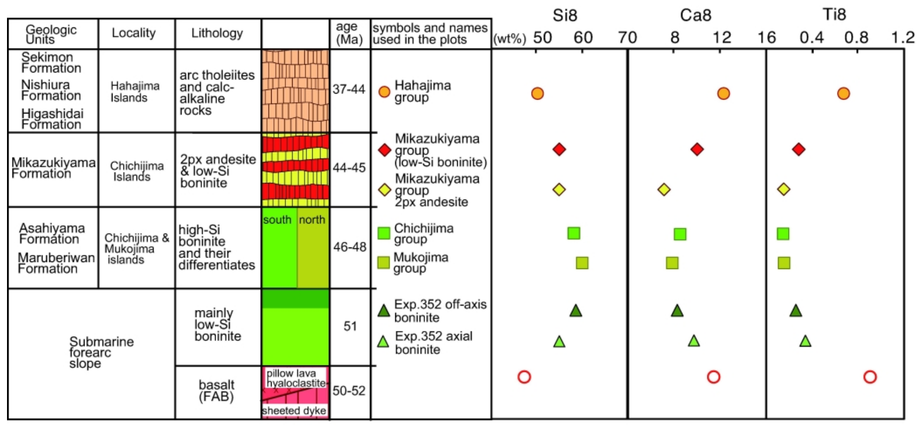

Fig. 2 Ishizuka et al.

Fig. 2. Schematic stratigraphic section and overall chemostratigraphic variation through the Bonin Ridge forearc crust. Rock types and symbols show in this figure remain consistent through the geochemical plots in all figures. Average content of SiO_2, CaO and TiO_2 projected to 8% MgO (Si8, Ca8 and Ti8) for each stratigraphic unit are shown in the columns to the right.

196x252mm (600 x 600 DPI)

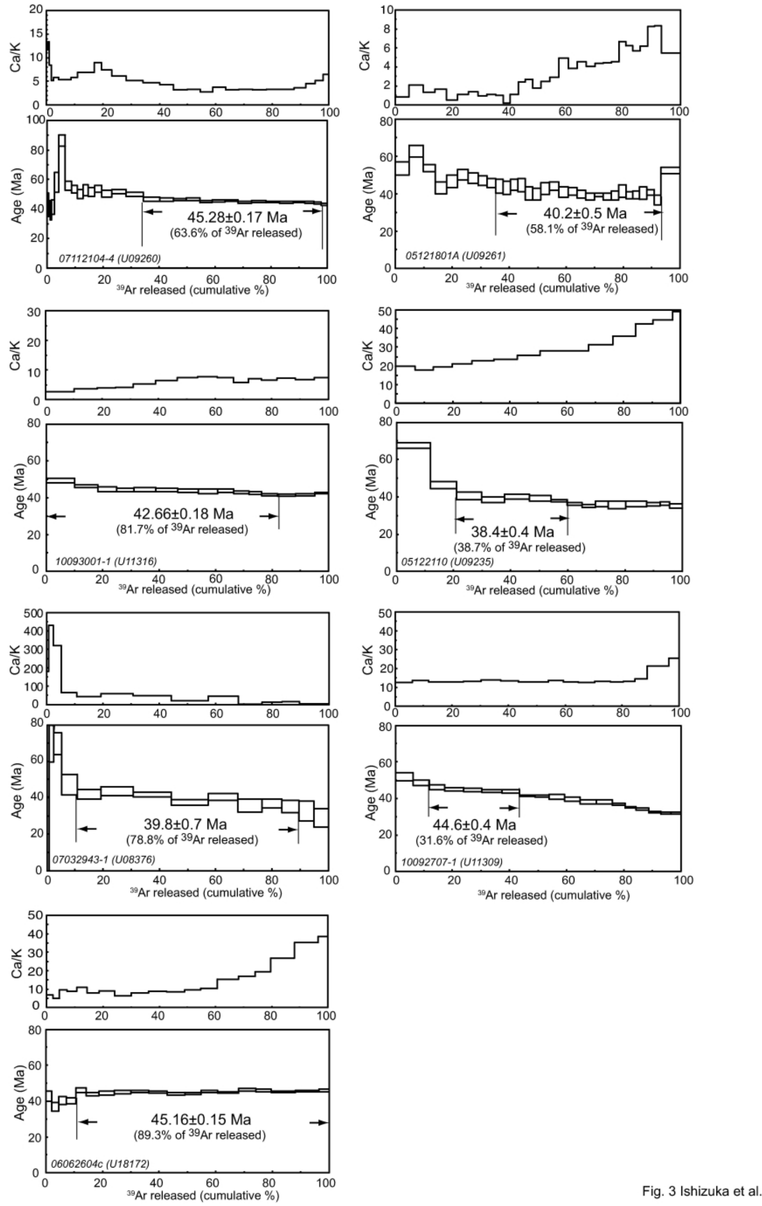

Fig. 3. 40Ar/39Ar age spectra and Ca/K plots for groundmass samples from the Bonin Islands.

177x281mm (600 x 600 DPI)

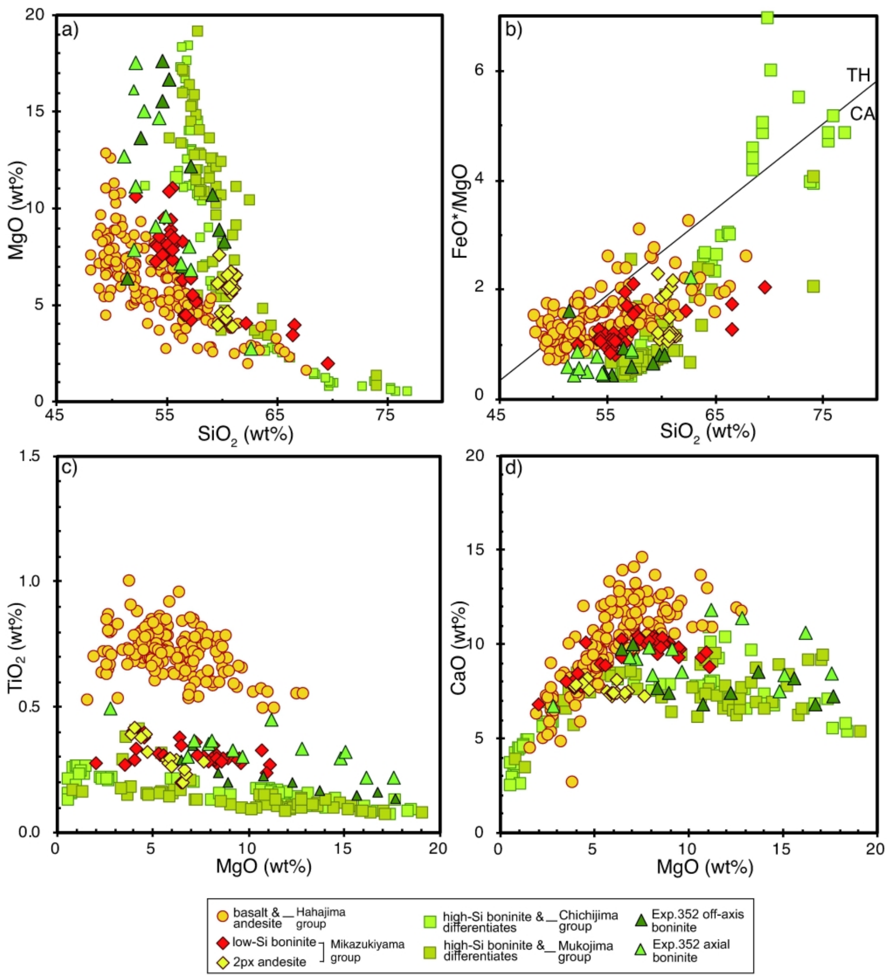

Fig. 4 Ishizuka et al.

Fig. 4. Major element composition of volcanic rocks from the Bonin Islands. Variation of SiO2 with a) MgO, b) FeO*(FeOtotal)/MgO (Line distinguishing the tholeiitic and calc-alkaline field is from Miyashiro (1974)), and variation of MgO with c) TiO2, and d) CaO. Data of boninites from IODP Exp. 352 are from Li et al. (2019).

186x253mm (600 x 600 DPI)

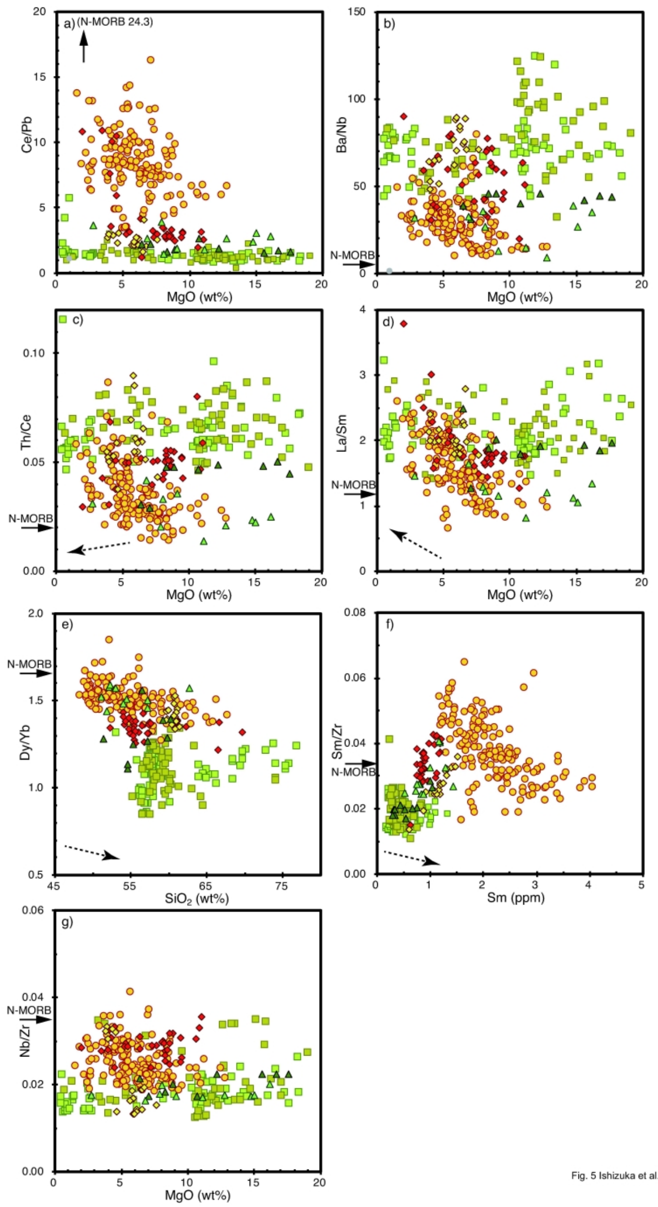

Fig. 5 Incompatible trace element ratios for the Bonin Islands. Variation of a) Ce/Pb, b) Ba/Nb, c) Th/Ce, d) La/Sm, e) Dy/Yb with SiO2 in wt%, f) Sm/Zr with Sm in ppm and g) Nb/Zr with MgO in wt%. Data of boninites from IODP Exp. 352 are from Li et al. (2019). Symbols as in Fig. 4. Average trace element ratios for all normal MORB (Gale et al., 2013) are shown. Dashed line with arrow in each plot (where the partition coefficient data is available) qualitatively show effect of fractionation of amphibole as a guide based on partition coefficients for basalt and andesite compiled in the GERM data base (https://earthref.org).

160x289mm (600 x 600 DPI)

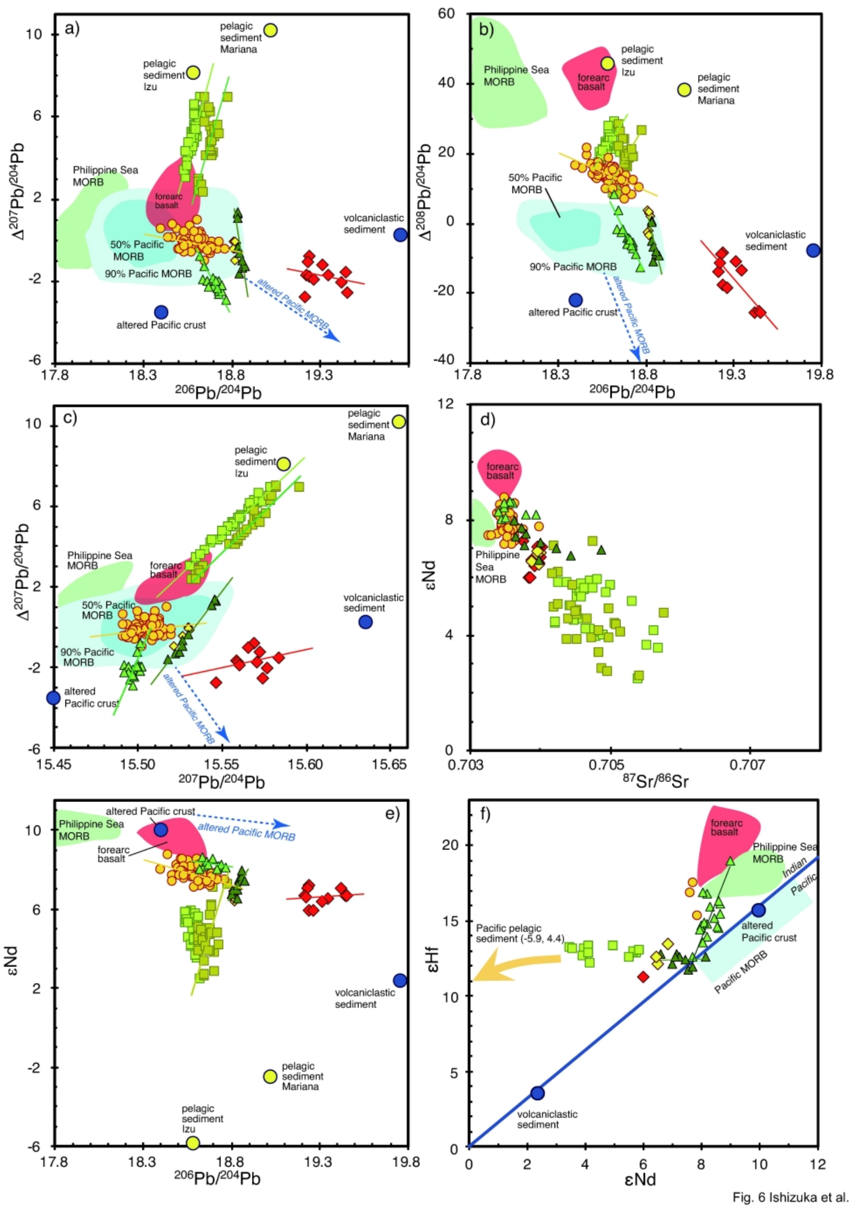

Fig. 6. Radiogenic isotope variation for the Bonin Islands plotted with potential slab and mantle components. a) Δ207Pb/204Pb vs. 206Pb/204Pb, b) Δ208Pb/204Pb vs. 206Pb/204Pb, c) Δ207Pb/204Pb vs. 207Pb/204Pb, d) εNd vs. 87Sr/86Sr, e) εNd vs. 206Pb/204Pb, f) εHf vs. εNd. Assumed compositions of subducting igneous crust and sediment are shown (Table S7). Pelagic sediment outboard of Izu-Bonin arc: Plank et al. (2007), Pelagic sediment outboard of Mariana arc: Plank & Langmuir (1998), Subducting altered igneous Pacific crust: Hauff et al. (2003), volcaniclastic sediment derived from HIMU oceanic islands: Plank & Langmuir (1998). Philippine Sea MORB: Hickey-Vargas (1991, 1998), Savov et al. (2006), Ishizuka et al. (2009, 2010, 2011b, 2013). Pacific MORB data was compiled from the Earthchem data base (https://www.earthchem.org). Least squares regression lines are shown in Pb isotopic plots for some rock types with sufficient data. Symbols are as on Fig. 4. Isotopic ratios plotted in these figures are not age-corrected.

205x289mm (600 x 600 DPI)

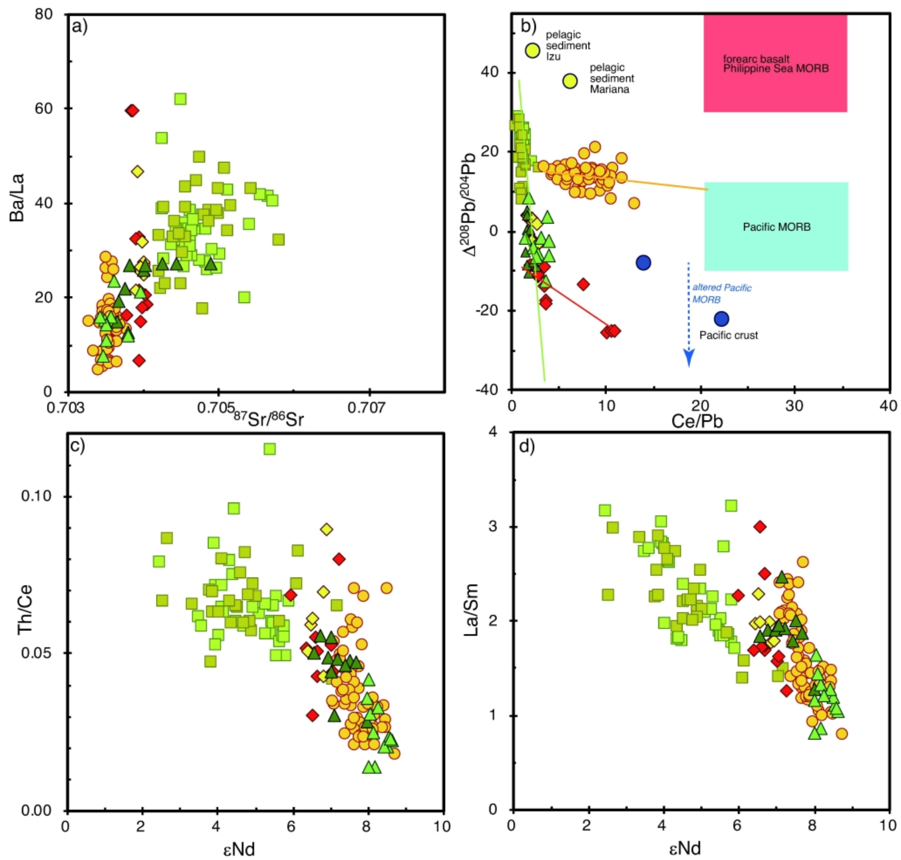

Fig. 7 Ishizuka et al.

Fig. 7. Isotope versus trace element ratio plots for the Bonin Islands volcanics. Data sources are the same as for Figure 6. Isotope versus trace element ratio plots for the Bonin Islands volcanics. Data sources are the same as for Figure 6. Least squares regression lines are shown in panel b. Symbols as in Fig. 4.

202x271mm (600 x 600 DPI)

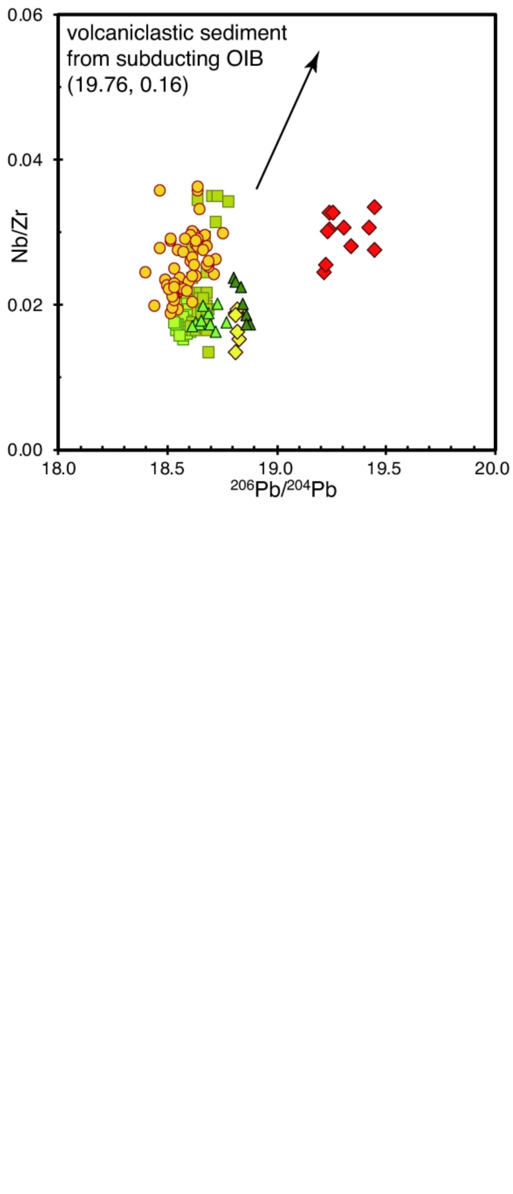

Fig. 8. Nb/Zr vs. 206Pb/204Pb plot. A vector towards volcaniclastic sediment derived from HIMU oceanic islands is shown (Plank & Langmuir, 1998). Symbols as in Fig. 4.

168x235mm (600 x 600 DPI)

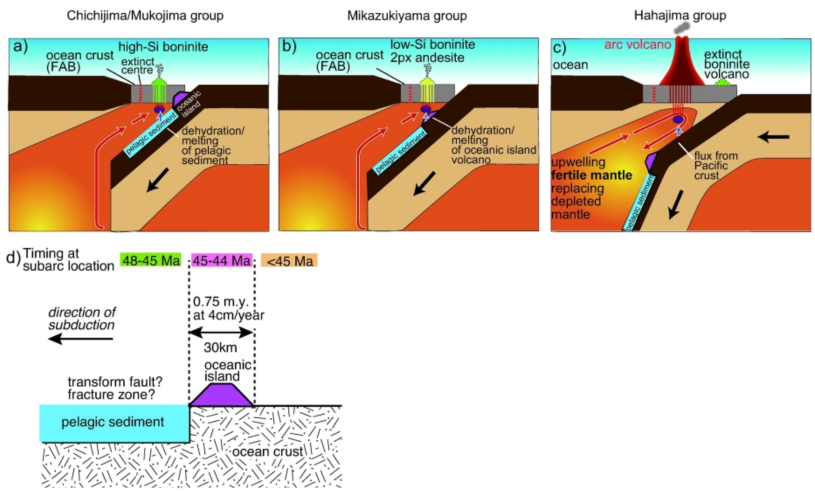

Fig. 9 Ishizuka et al.

Fig. 9. Schematic diagram showing the progressive variation in the nature of the slab flux following subduction initiation. a) Chichijima/Mukojima group, 48-45 Ma: shallow melting (~35 km) with flux from pelagic sediment and Pacific Ocean igneous crust added to a harzburgitic mantle; b) Mikazukiyama group, 45-44 Ma: melting at ~35 km, slightly further from the trench, flux from HIMU volcaniclastic sediment added to a less depleted mantle source; c) Hahajima group, <45 Ma: deeper melting (~60 km) further from the trench with flux from Pacific Ocean crust added to an upwelling, more fertile mantle source. d) Schematic diagram showing the estimated scale and duration of flux components on the subducting slab.

187x258mm (300 x 300 DPI)

Table 1 Results of $^{40}Ar/^{39}Ar$ dating of volcanic rocks from the Bonin islands.

Analysis No.	Sample No.	Name of island	steps	Total gas age (±1σ)	Plateau age (±1σ)				
				integrated age (Ma)	weighted average (Ma)	inv. isochron age (Ma)	$^{40}Ar/^{36}Ar$ intercept	MSWD	fraction of ^{39}Ar (%)
Hahajima Island Group									
09260	07112104-4	Hahajima	30	48.2±0.3	**45.28±0.17**	43.9±1.6	314±20	1.32	63.6
09261	05121801A	Hahajima	31	45.2±0.5	**40.2±0.5**	39.7±4.5	296±6	0.90	58.1
11316	10093001-1	Hahajima	15	44.16±0.25	**42.66±0.18**	41.4±0.5	592±85	1.16	81.7
09235	05122110	Meijima	15	42.0±0.4	**38.4±0.4**	35.2±2.1	340±28	0.73	38.7
08376	07032943-1	Imoutojima	14	40.2±0.9	**39.8±0.7**	38.7±1.2	334±26	1.18	78.8
11309	10092707-1	Mukoujima	19	41.2±0.3	**44.6±0.4**	42.8±1.3	348±37	0.57	31.6
low-Si boninite from Chichijima Island Group									
18172	06062604C	Otoutojima	19	44.57±0.19	**45.16±0.15**	45.3±0.3	292±6	1.24	89.3

inv. isochron age: inverse isochron age.

MSWD: mean square of weighted deviates ((SUMS/(n-2))^0.5) in York (1969).

Integrated ages were calculated using sum of the total gas released.

$\lambda_b=4.962\times10^{-10}y^{-1}$, $\lambda_e=0.581\times10^{-10}y^{-1}$, $^{40}K/K=0.01167\%$ (Steiger & Jager 1977).

Atmospheric $^{40}Ar/^{36}Ar$: 295.5